Functional Asplund's metrics for pattern matching robust to variable lighting conditions

Guillaume Noyel, Michel Jourlin

Functional Asplund's metrics for pattern matching robust to variable lighting conditions[☆]

Guillaume Noyel[a,b,*], Michel Jourlin[c,a,*]

[a] *International Prevention Research Institute (iPRI), 18 Chemin des Cuers, 69570 Dardilly Lyon-Ouest, France*
[b] *University of Strathclyde, Institute of Global Public Health, 16 Richmond Street, G11XQ Glasgow, United Kingdom*
[c] *Université Jean Monnet, Laboratoire Hubert Curien, UMR CNRS 5516,18 Rue du Professeur Benoît Lauras, 42000 Saint-Etienne, France*

Abstract

In this paper, we propose a complete framework to process images captured under uncontrolled lighting and especially under low lighting. By taking advantage of the Logarithmic Image Processing (LIP) context, we study two novel functional metrics: i) the LIP-multiplicative Asplund's metric which is robust to object absorption variations and ii) the LIP-additive Asplund's metric which is robust to variations of source intensity and exposure-time. We introduce robust to noise versions of these metrics. We demonstrate that the maps of their corresponding distances between an image and a reference template are linked to Mathematical Morphology. This facilitates their implementation. We assess them in various situations with different lightings and movements. Results show that those maps of distances are robust to lighting variations. Importantly, they are efficient to detect patterns in low-contrast images with a template acquired under a different lighting. [1]

Keywords: Logarithmic Image Processing, Mathematical Morphology, Grayscale pattern matching, Double-sided probing, Asplund's metric, Map of Asplund's distances, Robustness to lighting variations

1. Introduction

Metrics or their values, namely the distances, play a central role in image analysis as comparison tools. They possess strong mathematical properties

[☆]This research did not receive any specific grant from funding agencies in the public, commercial, or not-for-profit sectors. The authors have no conflict of interest.

[*]Corresponding author.
Email addresses: guillaume.noyel@i-pri.org (Guillaume Noyel), michel.jourlin@univ-st-etienne.fr (Michel Jourlin)
URL: https://orcid.org/0000-0002-7374-548X (Guillaume Noyel)

[1]Abbreviation: LIP (Logarithmic Image Processing).

(symmetry, separation, triangular inequality) but they are generally not founded on optical properties. They are therefore not adapted to the comparison of images captured under variable lighting conditions. This issue affects the most classical metrics like: the Euclidean-like distances [1, 2], the integral metric, the uniform metric, the Stepanov distance (or Minkowski distance) [3], the Hausdorff metric [4, 5] and many others [3]. The aim of this paper is to propose metric tools robust to lighting variations.

Let us present the issue we address. Many type of applications are affected by variable illumination, such as traffic control [6, 7], safety and surveillance [8], underwater vision [9, 10], driving assistance [11], face recognition [12, 13, 14, 15], large public health databases of images [16], etc. Let us summarise the difficulties inherent to this issue in the literature. E.g. Chen et al. [12] observe that the performance of classical techniques like gamma correction [17], logarithm transform [18], adaptive histogram equalisation [19], region-based histogram equalisation [17], and block-based histogram equalisation [20] present limitations. They propose a Discrete Cosine Transform in the logarithm domain [12]. Faraji and Qi [13] suggest other solutions based on logarithmic fractal dimension. Hussain Shah et al. [14] claim that: "Firstly, textural values are changed during illumination normalisation due to increase in the contrast that changes the original pixels of [images]. Secondly, it minimises the distance between inter-classes which increases the false acceptance rates". In [21], for unsharp masking algorithm or in [22] for retinex type of algorithms, the enhancement of noise is not taken into account. However, noise filtering is suggested in [21]. Consequently, the usual approach which consists of a pre-processing to normalise the illumination, significantly increases the difficulty to perform the second step dedicated to the recognition of a pattern. Moreover, the pre-processing is rarely based on a rigorous modelling of the cause of the lighting variations. We address this issue by proposing metric tools which are efficient in presence of lighting variations, without any pre-processing. Those metrics are especially robust to variations between low-contrast and high-contrast images. We start from a little-known metric defined for binary shapes [23, 24], namely the Asplund's metric. It consists of a double-sided probing of one of the shapes by the other. This binary metric has the outstanding property of being *insensitive to object magnification* [25]. Our motivation has been to extend this property to Asplund-like metrics dedicated to grey level images. Such extensions of the binary Asplund's metric to the functional case require the use of *homothetic images* or functions which are *insensitive to lighting variations*. Such a concept is mathematically well defined and physically justified in the Logarithmic Image Processing (LIP) framework [26, 27]. Two extensions will be studied: i) the LIP-multiplicative Asplund's metric based on the LIP-multiplication operation of an image by a real number and ii) the LIP-additive metric based on the LIP-addition operation of an image by a constant. A famous optical law, the Transmittance Law, is at the basis of both LIP-operations [27, chap. 1]. They give to the functional Asplund's metrics a strong physical property: a very low sensitivity to lighting variations, especially for under-lighted images. The LIP-multiplicative Asplund's metric is thereby theoretically insensitive to variations of the object

absorption (or opacity). The LIP-additive metric is defined to be insensitive to variations of source intensity (or exposure-time). For pattern matching purpose, a map of distances is computed between a template and an image. The closest image patterns to the template correspond to the minimal values of the map. The patterns are then detected by finding the map minima. In this paper, we will demonstrate that the maps of distances are related to the well established framework of Mathematical Morphology (MM) [28, 29, 30, 31]. This will facilitate their programming as numerous image analysis software contain these operations. Importantly, for the Asplund's metrics, there is no empirical preprocessing normalising the image intensity. Moreover, the consistency of the LIP model with Human Vision [32] allows the Asplund's metrics to perform pattern matching as a human eye would do. The link between these metrics and the LIP model opens the way to numerous applications with low-lighting [27].

In this paper, our aim is to present a complete framework of pattern matching robust to lighting variations between low-contrast and high-contrast images. In detail, our contribution is two-fold. (1) Firstly, we extend the preliminary works defining the functional metrics and their corresponding maps of distances between a template and an image [33, 25, 27, 34, 35, 36][2]. Beyond the prior work, we add theoretical work at two stages. a) We better define the robust to noise version of the metrics. b) We demonstrate the link between the maps of distances and the MM operations of dilation and erosion [29]. An expression will be given between each map of distances and those MM operations. (2) The second part of our contribution is to perform an extensive experimental validation of the metrics on simulated and on real images. We show that Asplund's metrics are efficient for pattern recognition in images captured with different lightings. This is especially the case for the imaging of moving objects, where the motion blur is avoided by shortening the camera exposure-time with the side effect of darkening the images (Fig. 11).

The paper is organised as follows. After presenting the related methods of double-sided probing, the novelty of our approach will be pointed out (Sec. 2). The background notions will be then introduced (Sec. 3). The properties of Asplund's metrics will be studied in the LIP-multiplicative case (Sec. 4) and in the LIP-additive case (Sec. 5). Experiments will illustrate the specific interest of each functional Asplund's metrics (Sec. 6). Demonstrations will be given in the appendix and in the supplementary materials.

2. Related works and novelty

2.1. Related Works

Pattern matching methods efficient under variable lighting conditions are seldom studied in the literature. This explains the few references closely related

[2] [35] is a personal communication which is unpublished.

to our work. Nevertheless, we can cite two papers of Barat et al. [37, 38]. The first one proposes the concept of probing in order to replace one of the following methods. (i) The morphological approach proposed by Banon and Faria [39]. (ii) The extension of the "hit-or-miss" transform [29] to grey-level images introduced by Khosravi and Schafer [40]. (iii) The approach inspired by the computation of Hausdorff distance of Odone et al. [41]. (iv) The multi-scale tree matching using boundary segments presented by Cantoni et al. [42]. In the second paper, Barat et al. introduced the double-sided probing of a grey level function f, where a pair of probes locally surrounds the representative surface of f. Such a technique detects the possible locations of the searched pattern. However, the probes are arbitrarily chosen and simply translated along the grey scale to remain in contact with the function f. These translations, which darken (or brighten) the probes, seem to take into account the lighting variations of the image. However, as they are not physically founded, they do not correctly model any of such variations.

2.2. Novelty of functional Asplund's metrics

The novelty of the functional Asplund's metrics is to be theoretically insensitive to lighting variations, with a physical origin. Unlike the related works, the functional Asplund's metrics use the LIP-multiplicative and LIP-additive laws to compare a given template to a studied grey level function f. Due to the LIP-laws, the template generates itself the pair of probes suited to the values of the function f. The arbitrary choice of the probes made by Barat et al. [38] is therefore avoided in our approach.

3. Background: From a metric for binary shapes to a metric for grey level images

Asplund's metric originally defined for binary shapes [23, 24], has been extended to grey-level images in the LIP-framework by Jourlin et al. [33, 25]. In this section, we give background notions about the binary Asplund's metric, the LIP model, the Functional Asplund's metrics and MM.

3.1. Asplund's metric for binary shapes

In the initial definition of Asplund's metric for a pair (A, B) of binary shapes, one shape, e.g. B, is chosen to perform the double-sided probing of A by means of two *homothetic* shapes of B. Two real numbers are computed: the smallest number λ_0 such that $\lambda_0 B$ contains A and the greatest number μ_0 such that A contains $\mu_0 B$. The Asplund's distance $d_{As}(A, B)$ between A and B is then defined according to:

$$d_{As}(A, B) \quad = \quad \ln(\lambda_0/\mu_0). \tag{1}$$

Remark 1. This implies that d_{As} remains unchanged when one shape is magnified or reduced by any ratio k.

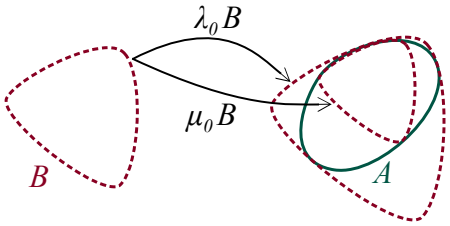

Figure 1: Asplund's metric for binary shapes. The shape A is probed on both sides by the reference shape B using its two homothetic shapes $\lambda_0 B$ and $\mu_0 B$.

Figure 1 illustrates the binary Asplund's metric where a shape A is probed on its both sides by a reference shape B.

The property of insensitivity to object magnification of the binary Asplund's metric can be extended to the functional case, where the functional Asplund's metric are insensitive to lighting variations. For this purpose, the LIP model is necessary.

3.2. Logarithmic Image Processing

The Logarithmic Image Processing (LIP) model has been introduced by Jourlin and Pinoli [43, 26]. A grey-level image f is defined on a domain $D \subset \mathbb{R}^n$ and takes its values in the grey scale $\mathcal{T} = [0, M[\subset \mathbb{R}$. f is an element of the set $\mathcal{I} = \mathcal{T}^D$. Contrary to common usage, the grey scale extremity 0 corresponds to the maximal possible intensity observed by the sensor (white), i.e. when no obstacle is located between the source and the sensor. The other extremity of the scale, M, corresponds to the limit case where no element of the source is transmitted (black). Such a limit value is excluded of the scale. For 8-bit digitised images, M is equal to 256. Now the two LIP operations on images can be defined: the addition of two images $f \mathbin{\triangle} g$ and the scalar multiplication $\lambda \mathbin{\triangle} f$ of an image by a real number λ. Both operations derive from the well-known *Transmittance Law* [27, chap. 1]: $T_{f \mathbin{\triangle} g} = T_f \times T_g$. The transmittance $T_f(x)$ of a grey level image f at a point x of D is the ratio of the out-coming flux at x by the incoming one. The incoming flux corresponds to the source intensity. From a mathematical point of view, the transmittance $T_f(x)$ represents the probability, for a particle of the source arriving in x to be seen by the sensor. The *Transmittance Law* $T_{f \mathbin{\triangle} g}$ means therefore that the probability of a particle to pass through the addition of two obstacles is nothing but the product of the probabilities to pass through each of them. The link, $T_f(x) = 1 - f(x)/M$, has been established in [26] between the grey level $f(x)$ and the transmittance $T_f(x)$. By replacing the transmittances T_f and T_g by their expressions in the expression of $T_{f \mathbin{\triangle} g}$, the LIP-addition of two images $f \mathbin{\triangle} g$ is obtained

$$f \mathbin{\triangle} g = f + g - fg/M. \tag{2}$$

Considering that the addition $f \mathbin{\overline{\wedge}} g$ may be written as $2 \mathbin{\overline{\wedge}} f$, the multiplication of an image f by a real number λ is then deduced from equation 2:

$$\lambda \mathbin{\overline{\wedge}} f = M - M\left(1 - f/M\right)^{\lambda}. \tag{3}$$

Remark 2. The opposite function $\overline{\triangle} f$ of f is easily obtained thanks to the equality $f \mathbin{\overline{\wedge}} (\overline{\triangle} f) = 0$, as well as the difference between two grey level functions f and g:

$$\overline{\triangle} f = (-f)/(1 - f/M) \tag{4}$$

$$f \mathbin{\overline{\triangle}} g = (f - g)/(1 - g/M). \tag{5}$$

Let us note that $\overline{\triangle} f$ is not an image (as it takes negative values) and $f \mathbin{\overline{\triangle}} g$ is an image if and only if $f \geq g$.

The LIP framework possesses the fundamental properties that are listed next.

Property 1 (The LIP framework is not limited to images in transmission)**.** *As the LIP model is consistent with Human Vision [32], the LIP operators are also valid for images acquired in reflected light and especially when a human interpretation of images is simulated.*

Property 2 (Strong physical properties)**.** *For images acquired in transmission, the LIP-addition (or subtraction) of a constant c to (or from) an image f consists of adding (or subtracting) a uniform half-transparent object of grey level c, which results in a darkening (or lightening) of f. Such operations are useful to correct illuminations variations. The images acquired in transmitted or reflected light have the two following properties.*

- *The addition (or subtraction) of a constant c to (or from) f simulates the decrease (or increase) of the acquisition exposure-time [44, 45]. If the values of $f \mathbin{\overline{\triangle}} c$ become strictly negative, they perform as light intensifiers [27, chap. 4].*
- *The scalar multiplication $\lambda \mathbin{\overline{\wedge}} f$ of f by a positive real number λ signifies that the thickness (or the absorption) of the half-transparent object which generates f is LIP-multiplied by λ. The image is darkened if $\lambda \geq 1$ or lightened if $\lambda \in [0, 1[$.*

Property 3 (Strong mathematical properties)**.** *Let $\mathcal{F}_M =]-\infty, M[^D$ be the space of functions defined on D with values in $]-\infty, M[$. $(\mathcal{F}_M, \overline{\wedge}, \overline{\wedge})$ is a real vector space and the space of images $(\mathcal{I}, \overline{\wedge}, \overline{\wedge})$ represents its positive cone [26, 27].*

In figure 2, several half-transparent sheets are stacked upon each others between a light source and a camera [46, 27]. The camera acquires an image of the light source through the sheets. The perceived intensity $f(x)$ by the camera, at a point x, is plotted as a function of the number of sheets. The inverted grey scale is used for the intensity axis. When there is no obstacle, the intensity is 0 (white). With the number of stacked sheets, it increases in a logarithmic

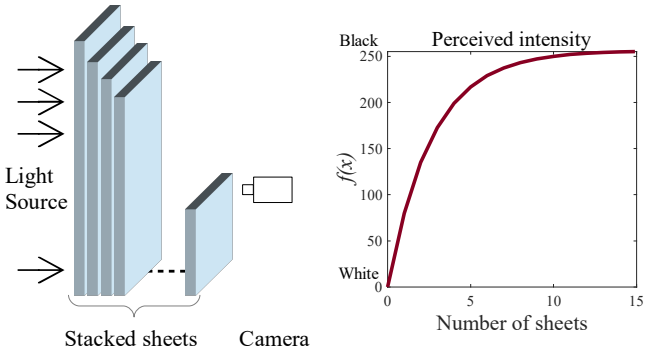

Figure 2: A light source passes trough several half-transparent sheets which are stacked. The perceived intensity $f(x)$ by the camera is plotted as a function of the sheet numbers using the inverted grey scale.

way and reaches a maximum M (black), when no light is perceived trough the sheets. The non-linearity of the perceived intensity is taken into account by the LIP model. Such a model will be useful to define functional Asplund's metrics with strong properties.

Remark 3. There exists a symmetric version of the LIP, namely the Symmetric LIP [47]. However, this model is not physically justified albeit it is interesting from a mathematical point of view for his symmetry. It allows e.g. to propose a LIP version of the Laplacian operator or to create Logarithmic Wavelets [48].

3.3. Definition of Functional Asplund's metrics

In this section, we will remind the LIP-multiplicative Asplund's metric. We will then clarify the definition and properties of the LIP-additive metric.

3.3.1. LIP-multiplicative Asplund's metric

Here, we will give the definition of the metric, one of its properties and a rigorous definition. Those were introduced by Jourlin et al. [33, 25], Noyel and Jourlin [34]. Let $\mathcal{T}^* =]0, M[$ be the grey-level axis without the zero value and $\mathcal{I}^* = \mathcal{T}^{*D}$ the space of images with strictly positive values.

Definition 1 (LIP-multiplicative Asplund's metric)**.** *Let f and $g \in I^*$ be two grey level images. As for binary shapes, we select a probing function, e.g. g, and we define the two numbers: $\lambda = \inf\{\alpha, f \leq \alpha \mathbin{\triangle} g\}$ and $\mu = \sup\{\alpha, \alpha \mathbin{\triangle} g \leq f\}$. The LIP-multiplicative Asplund's metric $d^{\triangle}_{As}$ is defined by:*

$$d^{\triangle}_{As}(f, g) \quad = \quad \ln(\lambda/\mu)\,. \tag{6}$$

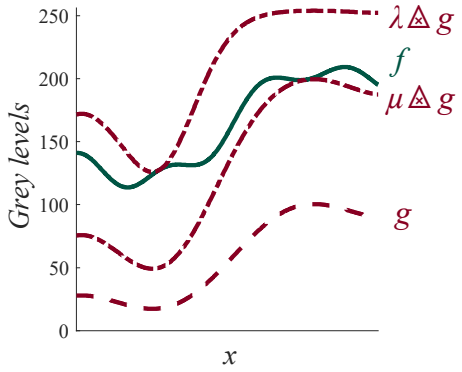

Figure 3: Double-sided probing of a function f by a probe g performed by the LIP-multiplicative Asplund's metric. $\mu \triangleq g$ is the lower probe and $\lambda \triangleq g$ is the upper probe.

Figure 3 illustrates the double-sided probing of image f by a probe g. The lower probe $\mu \triangleq g$ is in contact with the lower side of the function f whereas the upper probe $\lambda \triangleq g$ is in contact with the upper side of f. By comparison with the probe shape, the shapes of the lower and upper probes are deformed by the LIP-multiplication $\triangleq$. Such a deformation which depends on the grey value of g, is characteristic of the following metric property.

Property 4 (Invariance to LIP-multiplication)**.** *The strongest advantage of the LIP-multiplicative Asplund's metric is to remain unchanged when one image (e.g. f) is replaced by any homothetic $\alpha \triangleq f$, $\forall \alpha \in \mathbb{R}^{*+}$: $d^{\triangleq}_{As}(f,g) = d^{\triangleq}_{As}(\alpha \triangleq f, g)$.*

This latest equation demonstrates the insensitivity of the metric $d^{\triangleq}_{As}$ to illumination variations modelled by the LIP-multiplicative law $\triangleq$, i.e. those which correspond to an absorption change of the object.

Remark 4 (*Mathematical appendix [27, chap. 3]*). Considering the previous property, it would be more rigorous to explain the LIP-multiplicative Asplund's metric as follows.

a) An equivalence relation $\mathscr{R}$ is defined on the space of grey level images. Two images f and $g \in \mathcal{I}$ are said "in relation" if they satisfy: $(f \mathscr{R} g) \Leftrightarrow \exists \alpha > 0, \quad f = \alpha \triangleq g$. The previous relation $\mathscr{R}$ obviously satisfies the properties of an equivalence relation (reflexivity, symmetry and transitivity).

b) To each image $f \in \mathcal{I}^*$, its equivalence class $f^{\triangleq}$ is associated: $f^{\triangleq} = \{g,\ g \mathscr{R} f\}$.

c) A rigorous definition of the LIP-multiplicative Asplund's metric is then given into the space of equivalence classes $\mathcal{I}^{\triangleq}$ by: $\forall (f^{\triangleq}, g^{\triangleq}) \in (\mathcal{I}^{\triangleq})^2$, $d^{\triangleq}_{As}(f^{\triangleq}, g^{\triangleq}) = d^{\triangleq}_{As}(f_1, g_1)$. $d^{\triangleq}_{As}(f_1, g_1)$ is the Asplund's distance between any elements f_1 and g_1 of the equivalence classes $f^{\triangleq}$ and $g^{\triangleq}$.

3.3.2. LIP-additive Asplund's metric

As for the LIP-multiplicative metric, we will give a definition of the LIP-additive Asplund's metric, some properties and a rigorous definition.

Definition 2 (LIP-additive Asplund's metric)**.** *Let f and $g \in \mathcal{F}_M$ be two functions, we select a probing function, e.g. g, and we define the two numbers: $c_1 = \inf\{c, f \leq c \mathbin{\triangleq} g\}$ and $c_2 = \sup\{c, c \mathbin{\triangleq} g \leq f\}$, where c lies in the interval $]-\infty, M[$. The LIP-additive Asplund's metric $d^{\triangleq}_{As}$ is defined according to:*

$$d^{\triangleq}_{As}(f,g) \quad = \quad c_1 \mathbin{\triangle} c_2. \tag{7}$$

Remark 5. By definition, the values of c_1 and c_2 lie in the interval $]-\infty, M[$, which implies that the probing functions $g \triangle c_1$ and $g \triangle c_2$ are not always images. However, c_1 is always greater than c_2. Nevertheless, the Asplund's metric as the following property.

Proposition 1. *$d^{\triangleq}_{As}(f,g)$ lies in $[0, M[$ (Proof p. 29).*

Property 5 (Invariance to LIP-addition)**.** *The LIP-additive Asplund's metric remains unchanged when $f \in \mathcal{F}_M$ (or g) is replaced by any "translated" function $f \mathbin{\triangleq} k$, with $k \in]-\infty, M[$. Indeed, the constants c_1 and c_2 become $c_1 \mathbin{\triangleq} k$ and $c_2 \mathbin{\triangleq} k$ respectively. This implies that $d^{\triangleq}_{As}(f \mathbin{\triangleq} k, g) = d^{\triangleq}_{As}(f,g)$ and that $\forall f, \forall k, d^{\triangleq}_{As}(f, f \mathbin{\triangleq} k) = 0$. Knowing that the addition of a constant to a function is equivalent to a variation of exposure-time [44, 45], we have the fundamental result: the LIP-additive Asplund's metric is insensitive to exposure-time changing.*

Remark 6 (*Mathematical appendix*). As for the LIP-multiplicative Asplund's metric a rigorous mathematical definition is obtained by replacing each image f by its equivalence class $f^{\triangleq}$, which represents the set of functions h such that $h = f \mathbin{\triangleq} k$, for a constant k lying in $]-\infty, M[$. Nevertheless, if we keep the notations f and g, there is no ambiguity. Indeed, for a couple $(f^{\triangleq}, g^{\triangleq})$ of equivalence classes, we have $d^{\triangleq}_{As}(f^{\triangleq}, g^{\triangleq}) = d^{\triangleq}_{As}(f_1, g_1)$, where f_1 and g_1 are elements of the classes $f^{\triangleq}$ and $g^{\triangleq}$ respectively.

3.4. Fundamental operations in Mathematical Morphology

As the definition of functional Asplund's metrics is based on extrema between functions, there exists a natural link with MM as shown by Noyel and Jourlin [34]. MM [28, 29, 49, 50, 51, 31, 52] is defined in complete lattices [29, 53]. Let us recall some important definitions.

Definition 3 (Complete lattice)**.** *Given a set $\mathscr{L}$ and a partial order $\leq$ on $\mathscr{L}$, $\mathscr{L}$ is a complete lattice if every subset $\mathscr{X}$ of $\mathscr{L}$ has an infimum (a greatest lower bound) and a supremum (a least upper bound).*

The infimum and the supremum of $\mathscr{X}$ will be denoted by $\wedge\mathscr{X}$ and $\vee\mathscr{X}$, respectively. Two elements of the complete lattice $\mathscr{L}$ are important: the least element O and the greatest element I. E.g. the set of images from D to $[0, M]$, $\overline{\mathcal{I}} = [0, M]^D$, is a complete lattice with the partial order relation $\leq$. The least and greatest elements are the constant functions f_0 and f_M whose values are equal to 0 and M, respectively, for all the elements of D. The supremum and infimum are defined by taking the pointwise infimum and supremum, respectively. For $\mathscr{X} \subset \overline{\mathcal{I}}$, we have $(\wedge_{\overline{\mathcal{I}}}\mathscr{X})(x) = \wedge_{[0,M]}\{f(x) : f \in \mathscr{X},\ x \in D\}$ and $(\vee_{\overline{\mathcal{I}}}\mathscr{X})(x) = \vee_{[0,M]}\{f(x) : f \in \mathscr{X},\ x \in D\}$. Given $\overline{\mathbb{R}} = \mathbb{R} \cup \{-\infty, +\infty\}$, the set of functions $\overline{\mathbb{R}}^D$ is also a complete lattice with the usual order $\leq$.

Definition 4 (Erosion, dilation [53])**.** *Given $\mathscr{L}_1$ and $\mathscr{L}_2$ two complete lattices, a mapping $\psi \in \mathscr{L}_2^{\mathscr{L}_1}$ is*

- *an erosion ε: iff $\forall \mathscr{X} \subset \mathscr{L}_1$, $\psi(\wedge\mathscr{X}) = \wedge\psi(\mathscr{X})$;*
- *a dilation δ: iff $\forall \mathscr{X} \subset \mathscr{L}_1$, $\psi(\vee\mathscr{X}) = \vee\psi(\mathscr{X})$.*

As the definitions of these mappings apply even to the empty subset of $\mathscr{L}_1$, we have: $\varepsilon(I) = I$ and $\delta(O) = O$.

A structuring function b is a function defined on the domain $D_b \subset D$ with its values in $\overline{\mathcal{T}} = \overline{\mathbb{R}}$, or in $\overline{\mathcal{T}} = [0, M]$. In the case of a dilation or an erosion of a function f by an additive structuring function b, which is invariant under translation in the domain D, the previously defined dilation δ or erosion ε can be expressed in the same lattice $(\overline{\mathbb{R}}^D, \leq)$, or $(\overline{\mathcal{I}}, \leq)$ [54, 49] by:

$$(\delta_b(f))(x) = \vee_{h \in D_b}\{f(x - h) + b(h)\} = (f \oplus b)(x) \tag{8}$$

$$(\varepsilon_b(f))(x) = \wedge_{h \in D_b}\{f(x + h) - b(h)\} = (f \ominus b)(x) \tag{9}$$

The symbols $\oplus$ and $\ominus$ represent the extension to functions [29] of Minkowski operations between sets [29]. The term "additive structuring function" refers to a vertical translation in the image space $\overline{\mathcal{T}}$ [49].

4. Pattern analysis with LIP-multiplicative Asplund's metric

The LIP-multiplicative Asplund's metric is of utmost importance for pattern matching of objects whose absorption (or opacity) is varying. For this purpose, Jourlin et al. [33] introduced a map of LIP-multiplicative Asplund's distances. Noyel and Jourlin [55] studied it and Noyel and Jourlin [34, 35] established its link with MM through different conference papers. In this section, we will remind its definition, we will improve the definition of its robust to noise version and we will clearly present the link with MM.

4.1. Map of Asplund's distances

Let $\mathcal{T} = [0, M[$, $\mathcal{T}^* =]0, M[$ be grey-level axes and $\mathcal{I}^* = \mathcal{T}^{*D}$, $D \in \mathbb{R}^n$ the space of strictly positive images.

Definition 5 (Map of LIP-multiplicative Asplund's distances [33])**.** *Let $f \in \mathcal{I}^*$ be a grey-level image and $b \in (\mathcal{T}^*)^{D_b}$ a probe. The map of Asplund's distances $As_b^{\triangleq} : \mathcal{I}^* \to (\mathbb{R}^+)^D$ is defined by:*

$$As_b^{\triangleq} f(x) = d_{As}^{\triangleq}(f_{|D_b(x)}, b). \tag{10}$$

For each point $x \in D$, the distance $d_{As}^{\triangleq}(f_{|D_b(x)}, b)$ is computed in the neighbourhood $D_b(x)$ centred in x and the template b is acting like a structuring element. $f_{|D_b(x)}$ is the restriction of f to $D_b(x)$. $As_b^{\triangleq} f : D \to \mathbb{R}^+$ is the map of Asplund's distances between the image f and the probe b.

Figure 4 illustrates the map of Asplund's distances with an image of a butterfly [56]. The image is coming from the Yahoo Flickr Creative Commons 100 Million Dataset [57]. The processing is performed on its luminance image f which is in grey levels even if the images are displayed in colours. In the luminance image f of the butterfly (Fig. 4a), a white spot is selected to serve as a probe b (Fig. 4b). The map of Asplund's distances $As_b^{\triangleq} f$ between the image f and the probe b (Fig. 4c) presents a minimum which corresponds to the probe we are looking for (Fig. 4d). A map of Asplund's distances allows therefore to find a reference pattern or probe within an image. However, as images may present acquisition noise, a robust to noise version of the metric is useful for pattern matching.

4.2. A robust to noise version

Asplund's metric is computed using extrema, which makes it sensitive to noise. To overcome this limitation, Jourlin et al. [25] have proposed an extension which removes from D the most penalising points. This idea is related to the *topology of the measure convergence* [58, chap. 4] in the context of grey-level images. As the image is digitised, the number of pixels lying in D is finite. The "measure" of a subset of D is linked to the cardinal of this subset, e.g. the percentage P of its elements related to the domain D (or a region of interest $R \subset D$).

We are looking for a subset D' of D, such that *i)* $f_{|D'}$ and $g_{|D'}$ are neighbours (for Asplund's metric) and *ii)* the complementary set $D \setminus D'$ of D' related to D is small-sized as compared to D. This last condition is written: $P(D \setminus D') = \frac{\#(D \setminus D')}{\#D} \leq p$, where p represents an acceptable percentage and $\#D$ the number of elements in D. A neighbourhood of the image $f \in \mathcal{I}$ can be defined thanks to a small positive real number ϵ as: $N_{P,d_{As}^{\triangleq},\epsilon,p}(f) = \{g \backslash \exists D' \subset D, d_{As}^{\triangleq}(f_{|D'}, g_{|D'}) < \epsilon \text{ and } P(D \setminus D') \leq p\}$.

The set D' corresponds to the noise pixels to be discarded. As these pixels are the "closest" to the probe, they are selected by a function $\gamma_{(f,g)}^{\triangleq} : D \to \mathbb{R}$ characterising the (LIP-multiplicative) contrast between the functions f and g and which is defined by:

$$\forall x \in D,\ \gamma_{(f,g)}^{\triangleq}(x) \triangleq g(x) = f(x) \Leftrightarrow \gamma_{(f,g)}^{\triangleq} = \frac{\ln(1 - f/M)}{\ln(1 - g/M)}. \tag{11}$$

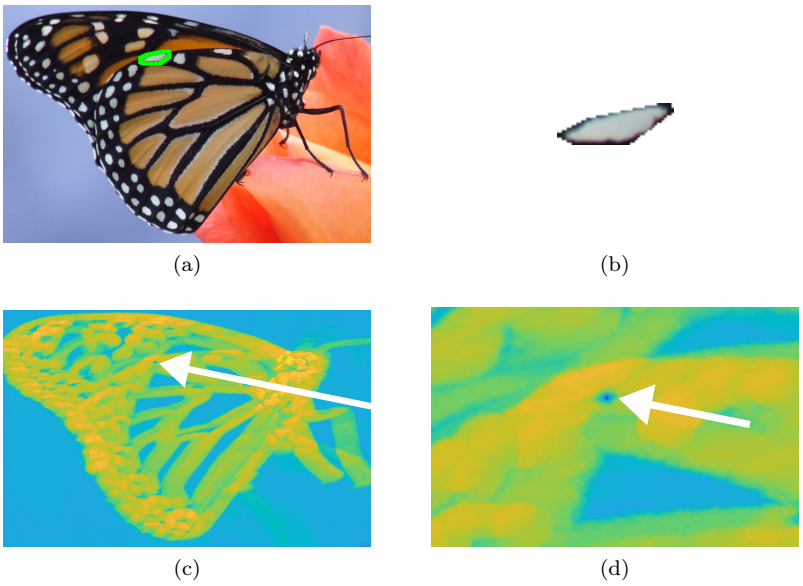

Figure 4: (a) Colour version of the butterfly image. In its luminance image f, a white spot - surrounded by the green curve - is selected as a probe function b. (b) Zoom in on the colour version of the luminance probe b. (c) Map of LIP-multiplicative Asplund's distances $As_b^{\triangleq} f$ between the image f and the probe b. Its minimum is indicated by the white arrow. (d) Zoom in on the map of Asplund's distances of the image. The white arrow points its minimum out.

$\gamma^{\triangleq}_{(f,g)}(x)$ is the real value by which each image value $f(x)$ is LIP-multiplied to be equal to the probe value $g(x)$. The expressions of the probes $\lambda \triangleq g$ and $\mu \triangleq g$ (Def. 1) can be written with the contrast function $\gamma^{\triangleq}_{(f,g)}$: $\lambda = \inf\{\alpha, \forall x, \gamma^{\triangleq}_{(f,g)}(x) \leq \alpha\}$ and $\mu = \sup\{\alpha, \forall x, \alpha \leq \gamma^{\triangleq}_{(f,g)(x)}\}$. This explains that the closest image values to the upper probe $\lambda \triangleq g$, or the lower probe $\mu \triangleq g$, correspond to the greatest, or smallest, values of $\gamma^{\triangleq}_{(f,g)}$, respectively. Using this property, new probes $\lambda' \triangleq g$, or $\mu' \triangleq g$, can be defined on the domain $D \setminus D'$ obtained by discarding a percentage $(1-p)/2$ of the pixels with the greatest, or smallest, contrast values $\gamma^{\triangleq}_{(f,g)}(x)$, respectively. The restricted domain $D \setminus D'$ has thereby a cardinal equal to a percentage p of the cardinal of D.

Definition 6 (LIP-multiplicative Asplund's metric with tolerance)**.** *Let* $(1-p)$ *be a percentage of points of* D *to be discarded and* D' *the set of these discarded points. The (LIP-multiplicative) Asplund's metric with tolerance between two grey-level images* f *and* $g \in \mathcal{I}$ *is defined by:*

$$d^{\triangleq}_{As,p}(f,g) = \ln(\lambda'/\mu'). \tag{12}$$

The factors λ' *and* μ' *are equal to* $\lambda' = \inf\{\alpha, \forall x \in D,\ \gamma^{\triangleq}_{(f_{|D\setminus D'}, g_{|D\setminus D'})}(x) \leq \alpha\}$ *and* $\mu' = \sup\{\alpha, \forall x \in D, \alpha \leq \gamma^{\triangleq}_{(f_{|D\setminus D'}, g_{|D\setminus D'})}(x)\}$*. A percentage* $(1-p)/2$ *of the*

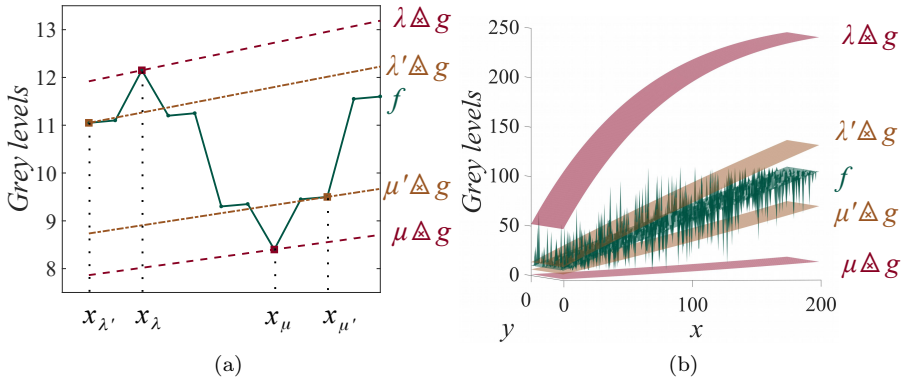

Figure 5: LIP-multiplicative Asplund's metric where g is used to probe f. $\lambda \triangleq g$ (respectively $\lambda' \triangleq g$) is the upper probe and $\mu \triangleq g$ (resp. $\mu' \triangleq g$) is the lower probe of the Asplund's metric $d^{\triangleq}_{As}(f,g)$ (resp. of the Asplund's metric with a tolerance p, $d^{\triangleq}_{As,p}(f,g)$). (a) Without tolerance, the Asplund's metric is equal to $d^{\triangleq}_{As}(f,g) = 0.42$ whereas with a tolerance $p = 80\%$ it decreases to $d^{\triangleq}_{As,p}(f,g) = 0.24$. (b) The image f is obtained by adding to the probe g a Gaussian white noise of mean 0, variance 5 and spatial density $\rho = 8\%$.

points $x \in D$ with the greatest, respectively lowest, contrast values $\gamma^{\triangleq}_{(f,g)}(x) = \frac{\ln(1-f(x)/M)}{\ln(1-g(x)/M)}$ are discarded.

Using equations 11 and 3, the contrast function $\gamma^{\triangleq}_{(f,g)}$ is proportional to the contrast function $\gamma^{\triangleq}_{(f,\alpha\triangleq g)}$ between the image f and the LIP-multiplied probe $\alpha \triangleq g$: $\gamma^{\triangleq}_{(f,\alpha\triangleq g)}(x) = (1/\alpha)\gamma^{\triangleq}_{(f,g)}(x)$, with $\alpha > 0$. This leads to the following property which is demonstrated in the supplementary materials.

Property 6. *The metric $d^{\triangleq}_{As,p}$ is invariant to the LIP-multiplication.*

Remark 7. A map of Asplund's distances with tolerance can be defined as in definition 5: $As^{\triangleq}_{b,p} f(x) = d^{\triangleq}_{As,p}(f_{|D_b(x)}, b)$.

Figure 5a illustrates the ability of the Asplund's metric with tolerance to discard the extremal values $f(x_\lambda)$ and $f(x_\mu)$ associated to noise. In figure 5b, the probe g is chosen as a plane and the image f is obtained by adding a noise to the probe with a spatial density of $\rho = 8\%$. The plane of the probe g is distorted by the LIP-multiplication used for the upper probe $\lambda \triangleq g$ and for the lower probe $\mu \triangleq g$. The Asplund's distance which is initially equal to $d^{\triangleq}_{As}(f,g) = 3.75$ decreases to $d^{\triangleq}_{As,p}(f,g) = 0.79$, with a tolerance of $p = 97\%$. Experiments have shown that with $p = 90\%$ ($\leq (1-\rho)$), the Asplund's distance is equal to zero.

4.3. Link with Mathematical Morphology

We first present the maps of distances with neighbourhood operations. We then establish the link with MM in the specific case of a flat structuring element and in the general case of a structuring function.

4.3.1. General expression of the map of Asplund's distances with neighbourhood operations

From equation 6, for each $x \in D$, there is $d^{\triangleq}_{As}(f_{|D_b(x)}, b) = \ln(\lambda_b f(x)/\mu_b f(x))$ with $\lambda_b f(x) = \inf\left\{\alpha, f_{|D_b(x)} \leq \alpha \triangleq b\right\}$ and $\mu_b f(x) = \sup\left\{\alpha,\ \alpha \triangleq b \leq f_{|D_b(x)}\right\}$. These expressions show that the map of Asplund's distances consists of a double-sided probing, at each point x, by the least upper bound $\lambda(x) \triangleq b$ and by the greatest lower bound $\mu(x) \triangleq b$. As $\lambda_b f(x)$ and $\mu_b f(x)$ exist for all $x \in D$, the following maps can be defined [34].

Definition 7 (LIP-multiplicative maps of the least upper and of the greatest lower bounds [34])**.** *Given $\overline{\mathbb{R}}^+ = [0, +\infty]$, let $f \in \overline{\mathcal{I}}$ be an image and $b \in (\mathcal{T}^*)^{D_b}$ a probe. Their map of the least upper bounds (mlub) $\lambda_b : \overline{\mathcal{I}} \to (\overline{\mathbb{R}}^+)^D$ and their map of the greatest lower bounds (mglb) $\mu_b : \overline{\mathcal{I}} \to (\overline{\mathbb{R}}^+)^D$ are defined by:*

$$\lambda_b f(x) = \inf_{h \in D_b} \{\alpha, f(x+h) \leq \alpha \triangleq b(h)\}, \tag{13}$$

$$\mu_b f(x) = \sup_{h \in D_b} \{\alpha, \alpha \triangleq b(h) \leq f(x+h)\}. \tag{14}$$

Let us define $\tilde{f} = \ln(1 - f/M)$, $f \in \overline{\mathcal{I}}$ and introduce the general expression of the mlub and of the mglb. The propositions 2 to 4 are demonstrated in [34] and in the supplementary materials. The proposition 5 is demonstrated in the Appendix A.1.

Proposition 2. *The mlub λ_b and mglb μ_b are equal to:*

$$\lambda_b f(x) = \vee\{\tilde{f}(x+h)/\tilde{b}(h), h \in D_b\}, \tag{15}$$

$$\mu_b f(x) = \wedge\{\tilde{f}(x+h)/\tilde{b}(h), h \in D_b\}. \tag{16}$$

Corollary 1. *Given $f \in \overline{\mathcal{I}}$, $f > 0$, the map of LIP-multiplicative Asplund's distances becomes:*

$$As^{\triangleq}_b f = \ln\left(\frac{\lambda_b f}{\mu_b f}\right). \tag{17}$$

4.3.2. Particular case of a flat structuring element

In the case of a flat structuring element, the expressions of the different maps can be simplified as follows.

Proposition 3. *Let $b = b_0 \in (\mathcal{T}^*)^{D_b}$ be a flat structuring element ($\forall x \in D_b$, $b(x) = b_0$). The mlub λ_{b_0}, the mglb μ_{b_0} and the map of Asplund's distances $As^{\triangleq}_{b_0}$ are equal to:*

$$\lambda_{b_0} f = (1/\tilde{b}_0) \ln\left(1 - (\delta_{\overline{D}_b} f)/M\right) \tag{18}$$

$$\mu_{b_0} f = (1/\tilde{b}_0) \ln\left(1 - (\varepsilon_{D_b} f)/M\right) \tag{19}$$

$$As^{\triangleq}_{b_0} f = \ln\left[\frac{\ln\left(1 - (\delta_{\overline{D}_b} f)/M\right)}{\ln\left(1 - (\varepsilon_{D_b} f)/M\right)}\right], \quad \textit{where } f > 0. \tag{20}$$

$\overline{D}_b = \{-h, h \in D_b\}$ *is the reflected (or transposed) domain of the structuring element.*

This result shows that the map of Asplund's distances is a combination of logarithms, an erosion ε_b and a dilation δ_b of the image f by the flat structuring element b. As numerous image processing libraries include erosion and dilation operations, the program implementation becomes easier.

4.3.3. General case: a structuring function

Proposition 4. *The mlub λ_b and the mglb μ_b are a dilation and an erosion, respectively, between the two complete lattices $\mathscr{L}_1 = (\overline{\mathcal{I}}, \leq)$ and $\mathscr{L}_2 = ((\overline{\mathbb{R}}^+)^D, \leq)$.*

Let us determine the expressions of this dilation and this erosion using MM with multiplicative structuring functions introduced by Heijmans and Ronse [49], Heijmans [30].

Definition 8 (Erosion and dilation with a multiplicative structuring function [49, 30])**.** *Given a function $f \in (\overline{\mathbb{R}}^+)^D$, and $b \in (\overline{\mathbb{R}}^+)^{D_b}$ a multiplicative structuring function:*

$$\vee_{h \in D_b} \{f(x-h).b(h)\} = (f \dot{\oplus} b)(x) \text{ is a dilation,} \tag{21}$$

$$\wedge_{h \in D_b} \{f(x+h)/b(h)\} = (f \dot{\ominus} b)(x) \text{ is an erosion,} \tag{22}$$

with the convention that $f(x-h).b(h) = 0$ when $f(x-h) = 0$ or $b(h) = 0$ and that $f(x+h)/b(h) = +\infty$ when $f(x+h) = +\infty$ or $b(h) = 0$. The symbols $\dot{\oplus}$ and $\dot{\ominus}$ represent the extension to multiplicative structuring functions of Minkowski operations between sets [29].

There exists a relation between the multiplicative erosion or dilation and the additive operations of section 3.4 [49, 30]:

$$f \dot{\oplus} b = \exp(\ln f \oplus \ln b), \tag{23}$$

$$f \dot{\ominus} b = \exp(\ln f \ominus \ln b). \tag{24}$$

The next proposition gives the morphological expressions of the different maps.

Proposition 5. *Let $b \in \mathcal{T}^{D_b}$ and $f \in \overline{\mathcal{I}}$, the expressions of the mlub λ_b, which is a dilation, and of the mglb μ_b, which is an erosion, are:*

$$\lambda_b f = (-\tilde{f}) \dot{\oplus} (-1/\tilde{\overline{b}}) = \exp(\hat{f} \oplus (-\hat{\overline{b}})), \tag{25}$$

$$\mu_b f = (-\tilde{f}) \dot{\ominus} (-\tilde{b}) \quad = \exp(\hat{f} \ominus \hat{b}). \tag{26}$$

$\overline{b}$ is the reflected structuring function defined by $\forall x \in \overline{D}_b$, $\overline{b}(x) = b(-x)$ [50] and $\tilde{f}$ is the function $\tilde{f} = \ln(1 - f/M)$, with $\tilde{f} \in [-\infty, 0]$. $\hat{f} = \ln(-\tilde{f}) = \ln(-\ln(1 - f/M))$ is a transform of f.

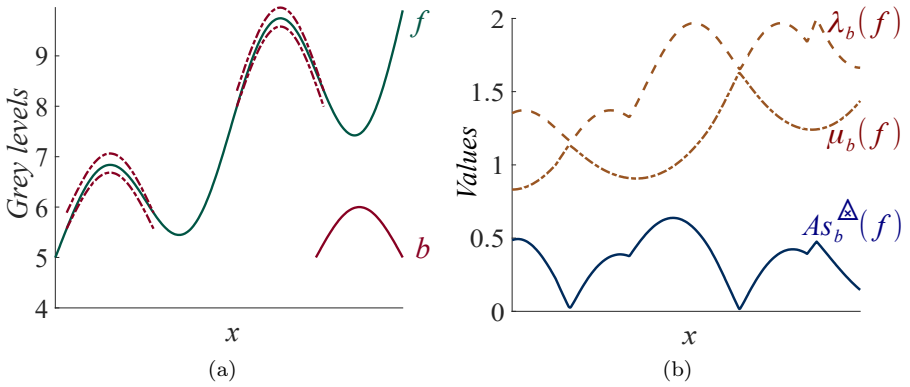

Figure 6: (a) The image f is probed on both sides by the probe b (in red colour) using the LIP-multiplicative law $\triangle$. The double-probing is depicted at two locations by the red dashed curves. (b) $\lambda_b f$ and $\mu_b f$ are the mlub and mglb of f, respectively. $As_b^{\triangle} f$ is the map of Asplund's distances between f and b.

The map of Asplund's distances is the difference between a dilation and an erosion whose expression is:

$$As_b^{\triangle} f = \left[\hat{f} \oplus (-\hat{\overline{b}})\right] - \left[\hat{f} \ominus \hat{b}\right] = \delta_{-\hat{\overline{b}}} \hat{f} - \varepsilon_{\hat{b}} \hat{f}. \tag{27}$$

We notice that the map of LIP-multiplicative Asplund's distances is similar to the (norm of the) morphological gradient $\varrho_{\hat{b}}$ or Beucher's gradient [54, 50]. It is the difference between a dilation and an erosion of the transformed image $\hat{f}$ by a structuring function $\hat{b}$: $\varrho_{\hat{b}} \hat{f} = \delta_{\hat{b}} \hat{f} - \varepsilon_{\hat{b}} \hat{f}$. This similarity shows that the map of Asplund's distances acts as an operator of derivation.

Remark 8. The map of Asplund's distances with tolerance $As_{b,p}^{\triangle}$ can be computed by replacing the dilation and erosion by rank-filters [54].

Figure 6a illustrates the double-sided probing of an image f by a probe b using the LIP-multiplicative law $\triangle$ which modifies the amplitude of the upper probes $\lambda_b f(x) \triangle b$ and of the lower probes $\mu_b f(x) \triangle b$. Both peaks have a different amplitude caused by a lighting drift created with the LIP-multiplicative law. In figure 6b, when the probe b is similar to a pattern in f (according to Asplund's distance), the map of Asplund's distances of f, $As_b^{\triangle} f$, presents a local minimum. Here, both peaks are located at the deepest minima of the map of f by the probe b, $As_b^{\triangle} f$. This result shows that the map of LIP-multiplicative Asplund's distances is insensitive to a lighting drift corresponding to a variation of absorption (or opacity) of the object.

5. Pattern analysis with LIP-additive Asplund's-like metric

The LIP-additive Asplund's metric is useful for images acquired with a small source intensity or a short exposure-time [27, chap. 3]. In this section, we will introduce: a map of LIP-additive Asplund's distances, a robust to noise version of the metric and the link between the map of distances and MM. Due to the important similarity with the LIP-multiplicative case (Sec. 4), we will only point out the new equations and results. We will consider the set of functions $\mathcal{F}_M = \mathcal{T}^D$ (or $\overline{\mathcal{F}}_M = \overline{\mathcal{T}}^D$) with values in $\mathcal{T} =]-\infty, M[$ (or $\overline{\mathcal{T}} = [-\infty, M]$).

5.1. Map of Asplund's distances

Definition 9 (Map of LIP-additive Asplund's distances)**.** *Let $f \in \mathcal{F}_M$ be a function and $b \in \mathcal{T}^{D_b}$ a probe. The map of Asplund's distances is the mapping $As_b^{\triangleq} : \mathcal{F}_M \to \mathcal{I}$ defined by:*

$$As_b^{\triangleq} f(x) = d_{As}^{\triangleq}(f_{|D_b(x)}, b). \tag{28}$$

The LIP addition $\triangleq$ makes the map of distances robust to contrast variations due to exposure-time changes.

5.2. A robust to noise version

In order to overcome the noise sensitivity of Asplund's metric, a neighbourhood $N_{P,d_{As}^{\triangleq},\epsilon,p}(f)$ of the function f is defined by replacing in section 4.2 the LIP-multiplicative Asplund's metric $d_{As}^{\triangleq}$ by the LIP-additive one $d_{As}^{\triangleq}$. The noise pixels which are the "closest" to the probe are selected by using a function $\gamma_{(f,g)}^{\triangleq} : D \to]-\infty, M[$ which characterises the (LIP-additive) contrast between the functions f and g:

$$\forall x \in D,\ \gamma_{(f,g)}^{\triangleq}(x) \triangleq g(x) = f(x) \Leftrightarrow \gamma_{(f,g)}^{\triangleq} = f \triangle g. \tag{29}$$

$\gamma_{(f,g)}^{\triangleq}(x) \in]-\infty, M[$ is the real value to be LIP-added to each function value $f(x)$ so that it becomes equal to the probe value $g(x)$. The expressions of the probes $c_1 \triangleq g$ and $c_2 \triangleq g$ (Def. 2) can be written with the contrast function: $c_1 = \inf\{c, \forall x, \gamma_{(f,g)}^{\triangleq}(x) \leq c\}$ and $c_2 = \sup\{c, \forall x, c \leq \gamma_{(f,g)}^{\triangleq}(x)\}$. This explains that the closest function values $f(x)$ to the upper probe $c_1 \triangleq g$, or the lower probe $c_2 \triangleq g$, correspond to the greatest, or smallest, values of $\gamma_{(f,g)}^{\triangleq}$, respectively. This property is used to introduce the following definition.

Definition 10 (LIP-additive Asplund's metric with tolerance)**.** *Let $(1-p)$ be a percentage of points of D to be discarded and D' the set of these discarded points. The LIP-additive Asplund's metric with tolerance between two functions f and $g \in \mathcal{F}_M$ is defined by:*

$$d_{As,p}^{\triangleq}(f,g) = c_1' \triangle c_2'. \tag{30}$$

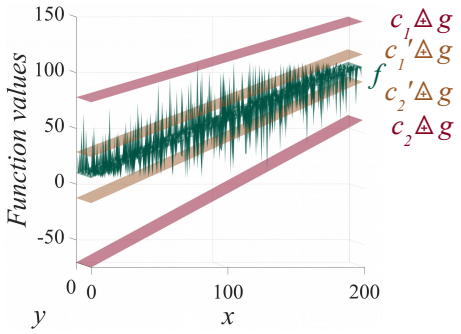

Figure 7: LIP-additive Asplund's metric for functions. g is used to probe f. $c_1 \triangleq g$ (respectively $c_1' \triangleq g$) is the upper probe and $c_2 \triangleq g$ (resp. $c_2' \triangleq g$) is the lower probe of the Asplund's metric $d^{\triangleq}_{As}(f,g)$ (resp. of the Asplund's metric with a tolerance p, $d^{\triangleq}_{As,p}(f,g)$). The function f is obtained by adding a Gaussian white noise to the planar probe g (mean 0, variance 5, spatial density $\rho = 8\%$).

The constants c_1' and c_2' are equal to: $c_1' = \inf\{c, \forall x \in D, \gamma^{\triangleq}_{(f_{|D\setminus D'}, g_{|D\setminus D'})}(x) \leq c\}$ *and* $c_2' = \sup\{c, \forall x \in D, c \leq \gamma^{\triangleq}_{(f_{|D\setminus D'}, g_{|D\setminus D'})}(x)\}$. *A percentage $(1-p)/2$ of the points $x \in D$ with the greatest, respectively lowest contrast values $\gamma^{\triangleq}_{(f,g)}(x) = f(x) \triangleq g(x)$ are discarded.*

From equations 29 and 5, the contrast function $\gamma^{\triangleq}_{(f,g)}$ is related to the contrast function $\gamma^{\triangleq}_{(f,c\triangleq g)}$, between f and the probe $c \triangleq g$, where $\forall x \in D, c(x) = c, c \in]-\infty, M[$, by the following equation: $\gamma^{\triangleq}_{(f,c\triangleq g)}(x) = \gamma^{\triangleq}_{(f,g)}(x) \triangleq c$. This leads to the following property demonstrated in the supplementary materials.

Property 7. *The metric $d^{\triangleq}_{As,p}$ is invariant to the LIP-addition of a constant.*

Remark 9. A map of Asplund's distances with tolerance can be introduced as in definition 9: $As^{\triangleq}_{b,p} f(x) = d^{\triangleq}_{As,p}(f_{|D_b(x)}, b)$.

Figure 7 illustrates the LIP-additive Asplund's metric robust to noise $d^{\triangleq}_{As,p}(f,g)$. The probe g is chosen as a plane and the function f is obtained by adding a noise to the probe g with a spatial density of $\rho = 8\%$. We notice that the upper probe $c_1 \triangleq g$ and the lower probe $c_2 \triangleq g$ may take negative values. After the LIP-addition, the planar surface of the probe g is still a plane, with a different orientation. The Asplund's distance which is is initially equal to $d^{\triangleq}_{As}(f,g) = 116$ decreases to $d^{\triangleq}_{As,p}(f,g) = 40$, with a tolerance $p = 97\%$. Experiments have shown that with $p = 90\%$ $(\leq (1-\rho))$, the Asplund's distance is equal to zero.

5.3. Link with Mathematical Morphology

5.3.1. General expression for the map of Asplund's distances with operations on neighbourhoods

In order to establish the link with MM, we will express the map of Asplund's distances with neighbourhood operations. From equation 7, for each $x \in D$, the

map expression becomes $d^{\triangleq}_{As}(f_{|D_b(x)}, b) = c_{1_b} f(x) \triangle c_{2_b} f(x)$, where $c_{1_b} f(x) = \inf\left\{c, f_{|D_b(x)} \leq c \triangleq b\right\}$ and $c_{2_b} f(x) = \sup\left\{c, c \triangleq b \leq f_{|D_b(x)}\right\}$. This leads to the following definition.

Definition 11 (LIP-additive maps of the least upper and of the greatest lower bounds)**.** *Let $f \in \overline{\mathcal{F}}_M$ be a function and $b \in \mathcal{T}^{D_b}$ a probe. Their map of the least upper bounds (mlub) $c_{1_b} : \overline{\mathcal{F}}_M \to \overline{\mathcal{F}}_M$ and their map of the greatest lower bounds (mglb) $c_{2_b} : \overline{\mathcal{F}}_M \to \overline{\mathcal{F}}_M$ are defined by:*

$$c_{1_b} f(x) = \inf_{h \in D_b} \{c, f(x+h) \leq c \triangleq b(h)\} \tag{31}$$

$$c_{2_b} f(x) = \sup_{h \in D_b} \{c, c \triangleq b(h) \leq f(x+h)\}. \tag{32}$$

The following propositions, 6 to 9, are demonstrated in the Appendix A.2. The general expressions of the mlub, mglb and map of distances will be given hereinafter.

Proposition 6. *The mlub c_{1_b} and the mglb c_{2_b} are equal to*

$$c_{1_b} f(x) = \vee \{f(x+h) \triangle b(h), h \in D_b\}, \tag{33}$$

$$c_{2_b} f(x) = \wedge \{f(x+h) \triangle b(h), h \in D_b\}. \tag{34}$$

Corollary 2. *The map of Asplund's distances between the function f and the probe b is equal to*

$$As^{\triangleq}_b f = c_{1_b} f \triangle c_{2_b} f. \tag{35}$$

5.3.2. Particular case of a flat structuring element

In the case of a flat structuring element, the expressions of the maps can be simplified as follows.

Proposition 7. *Let $b = b_0 \in \mathcal{T}^{D_b}$ be a flat structuring element ($\forall x \in D_b$, $b(x) = b_0$). The mlub $c_{1_{b_0}}$, mglb $c_{2_{b_0}}$ and map of Asplund's distances $As^{\triangleq}_{b_0}$ are equal to:*

$$c_{1_{b_0}} f = (\delta_{\overline{D}_b} f) \triangle b_0, \tag{36}$$

$$c_{2_{b_0}} f = (\varepsilon_{D_b} f) \triangle b_0, \tag{37}$$

$$As^{\triangleq}_{b_0} f = \delta_{\overline{D}_b} f \triangle \varepsilon_{D_b} f. \tag{38}$$

With a flat probe b, the map of Asplund's distances is a LIP difference between a dilation $\delta_{\overline{D}_b}$ and an erosion ε_{D_b} of the function f by the domain D_b of the structuring element b. It is similar to a morphological gradient with a LIP difference.

5.3.3. General case of a structuring function

The different mappings have the following morphological properties.

Proposition 8. *The mlub c_{1_b} (resp. mglb c_{2_b}) is a dilation (resp. an erosion) in the same lattice $\mathscr{L}_1 = \mathscr{L}_2 = \overline{\mathcal{F}}_M, \leq)$.*

Remark 10. In equation 35, one notice that the map of LIP-additive Asplund's distances is a LIP-difference between a dilation and an erosion, which corresponds to the LIP version of the morphological gradient. This similarity shows that the map of Asplund's distances acts as an operator of derivation.

Let us establish the relation between the dilation c_{1_b} or the erosion c_{2_b} with the dilation δ_b or the erosion ε_b (with an additive structuring function), respectively. For this purpose, a bijective mapping (i.e. an isomorphism) is needed between the lattice $\overline{\mathbb{R}}^D$ of $\delta_b f$, or $\varepsilon_b f$, and the lattice $\overline{\mathcal{F}}_M$ of $c_{1_b} f$, or $c_{2_b} f$. Jourlin and Pinoli [59], Navarro et al. [47] defined this isomorphism $\xi : \overline{\mathcal{F}}_M \to \overline{\mathbb{R}}^D$ and its inverse ξ^{-1} by:

$$\xi(f) = -M \ln (1 - f/M) \tag{39}$$

$$\xi^{-1}(f) = M(1 - \exp(-f/M)). \tag{40}$$

Remark 11. As ξ^{-1} and ξ are increasing bijections, they distribute over infima, as well as over suprema.

Proposition 9. *Given two functions $f, g \in \overline{\mathcal{F}}_M$, ξ has the property to transform the LIP-difference, $\triangle$, into the usual difference, $-$, $\xi(f \triangle g) = \xi(f) - \xi(g)$.*

The dilation c_{1_b} (eq. 33) and the erosion c_{2_b} (eq. 34) can therefore be expressed as:

$$\begin{aligned} c_{1_b} f(x) &= \xi^{-1} \circ \xi(\vee_{h \in \overline{D}_b} \left\{ f(x-h) \triangle \overline{b}(h) \right\} \\ &= \xi^{-1}[\vee_{h \in \overline{D}_b} \{\xi(f)(x-h) - \xi(\overline{b})(h)\}] \\ &= M(1 - e^{-\vee_{h \in \overline{D}_b} \{-\tilde{f}(x-h) + \tilde{\overline{b}}(h)\}}) \end{aligned} \tag{41}$$

$$\begin{aligned} c_{2_b} f(x) &= \xi^{-1}[\wedge_{h \in D_b} \{\xi(f)(x+h) - \xi(b)(h)\}] \\ &= M(1 - e^{-\wedge_{h \in D_b} \{-\tilde{f}(x+h)) - [-\tilde{b}(h)]\}}), \end{aligned} \tag{42}$$

where $\xi(f) = -M\tilde{f}$.

Proposition 10. *Let $b \in \mathcal{T}^{D_b}$ be a structuring function and $f \in \overline{\mathcal{F}}_M$ be a function. The expressions of their mlub c_{1_b}, which is a dilation, and of their mglb c_{2_b}, which is an erosion, are equal to:*

$$c_{1_b} f = \xi^{-1}[\xi(f) \oplus (-\xi(\overline{b}))] = M(1 - e^{-[\acute{f} \oplus (-\acute{\overline{b}})]}) \tag{43}$$

$$c_{2_b} f = \xi^{-1}[\xi(f) \ominus \xi(b)] \quad = M(1 - e^{-[\acute{f} \ominus \acute{b}]}). \tag{44}$$

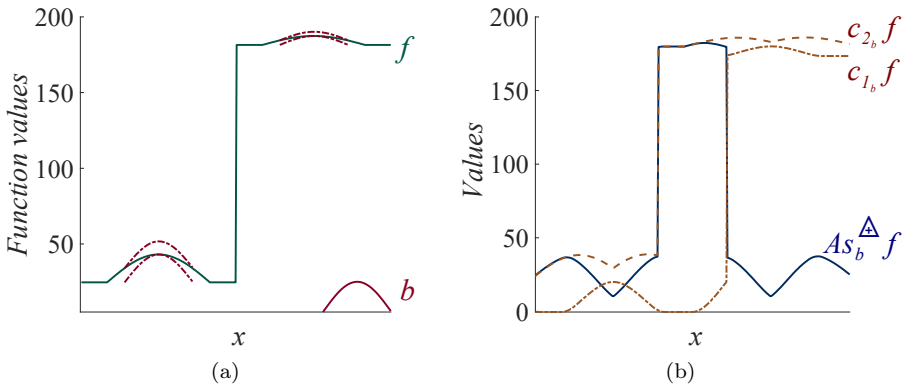

Figure 8: (a) The function f is probed on both sides (up and down) by the probe b (in red) using the LIP-additive law $\triangle$. The double-probing is depicted at two locations by the red dashed curves. (b) $c_{1_b} f$ and $c_{2_b} f$ are the mlub and the mglb of f, respectively. $As_b^{\triangle} f$ is the map of Asplund's distances between f and b.

$\acute{f} \in \overline{\mathbb{R}}^D$ *is a function defined by* $\acute{f} = -\tilde{f} = -\ln(1 - f/M) = [\xi(f)]/M$.

Their map of Asplund's distances is related to the difference between a dilation and an erosion (with an additive structuring function) by:

$$As_b^{\triangle} f = \xi^{-1}[(\xi(f) \oplus (-\xi(\bar{b}))) - (\xi(f) \ominus \xi(b))] \tag{45}$$

$$= M(1 - \exp(-[(\acute{f} \oplus (-\acute{\bar{b}})) - (\acute{f} \ominus \acute{b})])) \tag{46}$$

$$= M(1 - \exp(-[\delta_{-\acute{\bar{b}}} \acute{f} - \varepsilon_{\acute{b}} \acute{f}])).$$

Remark 12. By replacing the dilation and erosion by rank-filters [54] one can compute the map of Asplund's distances with a tolerance $As_{b,p}^{\triangle}$.

Figure 8a illustrates the double-sided probing of an image f by a probe (or structuring function) b. The amplitudes of both peaks are related by a LIP-addition of a constant. In figure 8b, the two deepest minima of the map of distances of f, $As_b^{\triangle} f$ correspond to the location of both peaks similar to the probe b. This illustrates the insensitivity of the map of LIP-additive Asplund's distances to a variation of light intensity or exposure-time.

6. Experiments and results

In this section, we will discuss the implementation of the maps of distances and we will illustrate them with simulated and real cases of image acquisition.

Table 1: Comparison between the durations of the morphological and direct implementations for the LIP-multiplicative map of Asplund's distances $As^{\triangleq}_b$, $As^{\triangleq}_{b,p=95\%}$ and the LIP-additive maps $As^{\triangleq}_b$ $As^{\triangleq}_{b,p=94\%}$. The example of figure 9 is used.

	$As^{\triangleq}_b f$	$As^{\triangleq}_{b,p=95\%} f$	$As^{\triangleq}_b f$	$As^{\triangleq}_{b,p=94\%} f$
Morphological	1.4 s	4.2 s	1.4 s	4.3 s
Direct	16.1 s	24.6 s	15.4 s	25.5 s
Gain factor	10.9	5.9	11.0	5.9

6.1. Implementation

The maps of LIP-multiplicative and LIP-additive Asplund's distances of the image f, $As^{\triangleq}_b f$ and $As^{\triangleq}_b f$, respectively, were both programmed in Matlab using their direct (eq. 10, 28) and morphological (eq. 27, 46) expressions. The same programming was done for the map of Asplund's distances with tolerance $As^{\triangleq}_{b,p} f$ and $As^{\triangleq}_{b,p} f$ of f. Due to the existence in numerous image analysis software (e.g. Matlab, Python scikit-images) of fast versions of the morphological operations $\oplus$ and $\ominus$ and of rank filters, the morphological implementation is easier and faster than the direct one. In table 1, the duration of the morphological and of the direct implementations (with parallelisation) of the maps of Asplund's distances without and with tolerance are compared using the example of figure 9. The image size is of 1224 $\times$ 918 pixels and the probe contains 285 pixels (Fig. 9d). The morphological implementation is always faster than the direct one, with a gain factor lying between 5.9 and 11 (processor Intel®Core$^{\text{TM}}$ i7 CPU 4702HQ, 2.20 GHz, 4 cores, 8 threads with 16Gb RAM).

6.2. Simulated cases

We evaluate the LIP-multiplicative and LIP-additive maps to detect balls in a bright image and in two darkened versions obtained by simulation (Fig. 9). The bright image is acquired in colour with "normal" contrasts - automatically selected by the camera (Fig. 9a) - and converted to a luminance image in grey-level, denoted f. A first darkened version $f_{dk,\triangleq}$ is obtained by the LIP-multiplication of f by a scalar λ (Fig. 9b). A second darkened version $f_{dk,\triangleq}$ is obtained by the LIP-addition of a constant k (Fig. 9e). Due to the light reflection at the surface of the balls and of other confounding objects, detecting the balls is a difficult task in these images. For this purpose, we used a probe b made of a ring surrounding a cylinder (Fig. 9d). The ring has an external radius of 15 pixels, a width of 3 pixels, a grey-level value of 18 and the disk has a radius of 2 pixels and a grey-level value of 190.

Remark 13. As the grey-scale is complemented in the LIP model, the LIP-multiplicative map $As^{\triangleq}_{b^c,p} f^c$ is computed using the image complement $f^c = M - f \in]0, M[^D$ and the probe complement b^c. However, the image $f_{dk,\triangleq} \in$

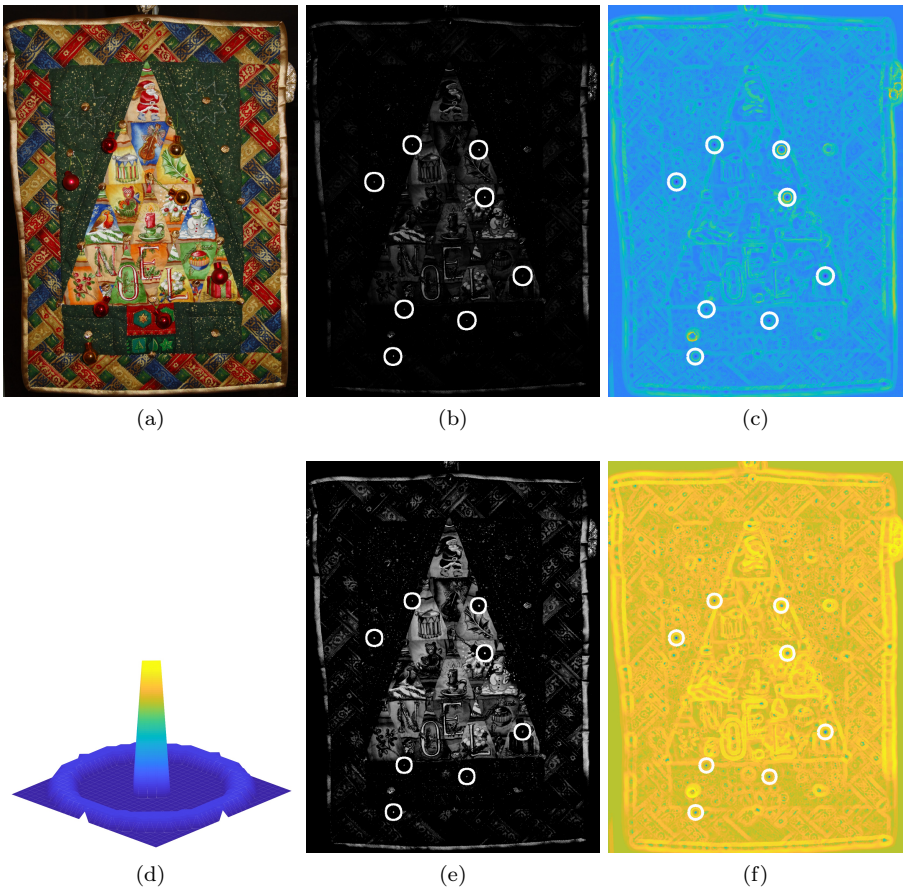

Figure 9: (a) Colour version of the luminance image f and (b) its darkened version $f_{dk,\triangleq} = (\lambda \triangleq f^c)^c$ obtained by the LIP-multiplication ($\lambda = 5$) of the complemented image luminance f^c. The balls are detected by a thresholding of (c) the map of LIP-multiplicative Asplund's distances of f^c with a tolerance $p = 95\%$, $As^{\triangleq}_{b^c,p} f^c$. (d) Probe b. (e) Darkened version $f_{dk,\triangleq} = k \triangleq f$ of the luminance image f obtained by the LIP-addition of $k = \triangleq 100 = -164.10$. The balls are segmented by a thresholding of (f) the map of LIP-additive Asplund's distances of f with a tolerance $p = 94\%$, $As^{\triangleq}_{b,p} f$.

$]-\infty, M[^D$, darkened by the LIP-addition of a constant, presents negative values and its complement $f^c_{dk,\triangleq} \in]0, +\infty[^D$ is outside of the dynamic range allowed for the map $[-\infty, M]^D$. For this reason, the darkened image $f_{dk,\triangleq}$ is not complemented.

In the image f (Fig. 9a) and in its darkened version $f_{dk,\triangleq}$ (Fig. 9b) obtained by LIP-multiplication, all the balls are detected by a thresholding of their map of Asplund's distances $As^{\triangleq}_{b^c,p} f^c$ (Fig. 9c). The map is the same for both images f and $f_{dk,\triangleq}$ because of its invariance to the LIP-multiplication. Similar results are

obtained for the image f (Fig. 9a), its darkened version $f_{dk,\triangleq}$ by LIP-addition (Fig. 9e) and their map of distances $As^{\triangleq}_{b,p}f$ (Fig. 9f) which is invariant to the LIP-addition. The same parameters of the probe were used for all the images f, $f_{dk,\triangleq}$ and $f_{dk,\triangleq}$. These results show that the maps of Asplund's distances are able to detect targets under different illumination conditions modelled by the LIP-multiplication $\triangleq$ or the LIP-addition $\triangleq$.

6.3. Real cases

The maps of LIP-additive and LIP-multiplicative Asplund's distances are then illustrated on real images. For a better visual interpretation, the results are presented with colour images even if the processing is made using their luminance.

6.3.1. LIP-additive metric: images acquired with a variable exposure-time

In figure 10, the same scene is captured with three different camera exposure-times (or shutter speeds). This gives three images with different brightnesses: a bright one f (Fig. 10a), a dark intermediate one f_{dk_1} (Fig. 10b) and a dark one f_{dk_2} (Fig. 10c). The scene is composed of bright balls on a multicolour background with other smaller balls acting as confounding objects. In order to make the ball detection more arduous, the camera is not exactly in the same position to capture the images. Moreover, the balls are of different colours, with different backgrounds and present several reflections. A disk of diameter 55 pixels is manually selected inside a ball of the bright image f (Fig. 10a) in order to serve as a probe function b. A map of Asplund's distances is computed between the complement of each of the three images and the same probe b using the same tolerance parameter $p = 70\%$. In the three distance maps of images $As^{\triangleq}_{b^c,p}f^c$ (Fig. 10d), $As^{\triangleq}_{b^c,p}f^c_{dk_1}$ (Fig. 10e) and $As^{\triangleq}_{b^c,p}f^c_{dk_2}$ (Fig. 10f), one can notice that the amplitudes are similar. This is caused by the low sensitivity of the LIP-additive Asplund's metric to lighting variations due to different exposure-times. In order to extract the location of the large balls, the maps of the dark intermediate image $As^{\triangleq}_{b^c,p}f^c_{dk_1}$ and of the dark image $As^{\triangleq}_{b^c,p}f^c_{dk_2}$ are segmented using the same technique - a thresholding (at 37^{th} percentile) and a reconstruction of the regional h-minima [50] - followed by a morphological post-processing (see remark in supplementary materials). Such a technique allows to detect all the large balls in both dark images f_{dk_1} (Fig. 10b) and f_{dk_2} (Fig. 10c), using the same probe b extracted in the bright image f (Fig. 10a). This illustrates the robustness of the map of LIP-additive Asplund's distances to different exposure-times.

The map of LIP-additive Asplund's distances is also useful to detect moving objects. In figure 11, a white disk with patterns is mounted on a turn table of a record player. The patterns include four small coloured disks and confounding shapes (i.e. eagles). First of all, an image f with good contrasts is captured with an appropriate exposure-time, 1/13 s (Fig. 11a). In this image, a circular probe b is selected inside a coloured disk. The record player is then started up at a speed of 45 tours/min and two images are captured. The first image $f_{mov,bl}$, which

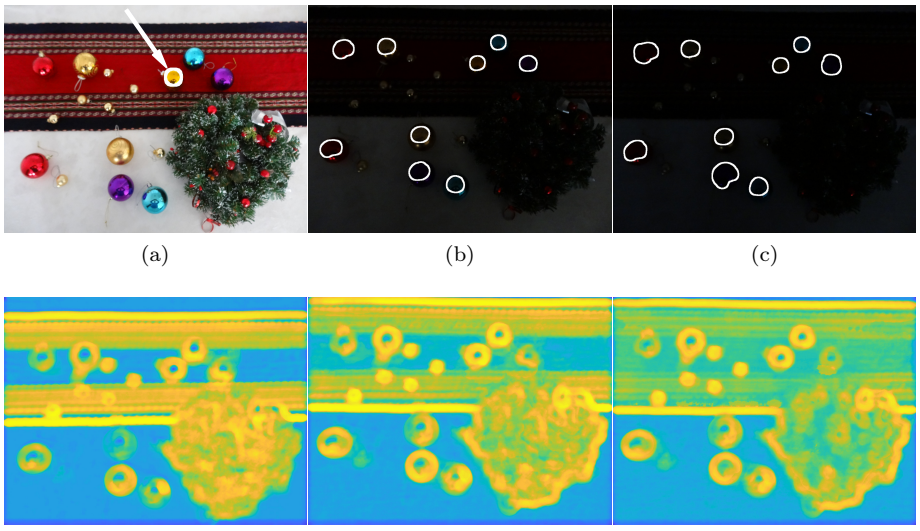

Figure 10: (a) Bright image f acquired with an exposure-time of 1/5 s. The probe function b is shown by the white arrow. (b) Ball detection in a dark intermediate image f_{dk_1} (exposure-time of 1/80 s). (c) Ball detection in a dark image f_{dk_2} (exposure-time of 1/160 s). (d) Map of LIP-additive Asplund's distances $As^{\triangleq}_{b^c,p} f^c$ of the image f, (e) map $As^{\triangleq}_{b^c,p} f^c_{dk_1}$ of the image f_{dk_1} and (f) map $As^{\triangleq}_{b^c,p} f^c_{dk_2}$ of the image f_{dk_2}. The tolerance parameter p is set to 70 %.

is acquired with the same exposure-time as the one of f, is correctly exposed but blurred (Fig. 11b). As it is blurred, it is useless to detect the coloured disks. A second image $f_{mov,dk}$ is acquired at a shorter exposure-time of 1/160 s. This second image is not blurred but darker than f (Fig. 11c). The map of LIP-additive Asplund's distances of its complement, $As^{\triangleq}_{b^c,p} f^c_{mov,dk}$ (Fig. 11e), is useful for the detection of the coloured disks. Those are detected by finding the regional minima of the map with sufficient height using the h-minima transform [50]. The regional minima with too large or too small area are also removed. By comparing the map of the moving disk image $As^{\triangleq}_{b^c,p} f^c_{mov,dk}$ (Fig. 11e) to the map of the fixed disk image $As^{\triangleq}_{b^c,p} f^c$ (Fig. 11d), one can notice that they both present similar shapes and amplitudes although the images f and $f_{mov,dk}$ are captured with different conditions. In particular, the kinetics of the scene are different because the disk is fixed or turning, and the lighting conditions differ significantly because the exposure-times are varying by a factor 12.

Figure 10 shows the robustness of the LIP-additive Asplund's metrics to intensity variations caused by variable exposure-times. Figure 11 shows its efficiency to detect moving objects in dark images acquired with a small exposure-time which is necessary to capture a fixed view of the object. Such cases occurs in many applications like medical images [16] or industry [60, 61]. E.g. in industrial control the objects are often presented to the camera on a conveyor (linear,

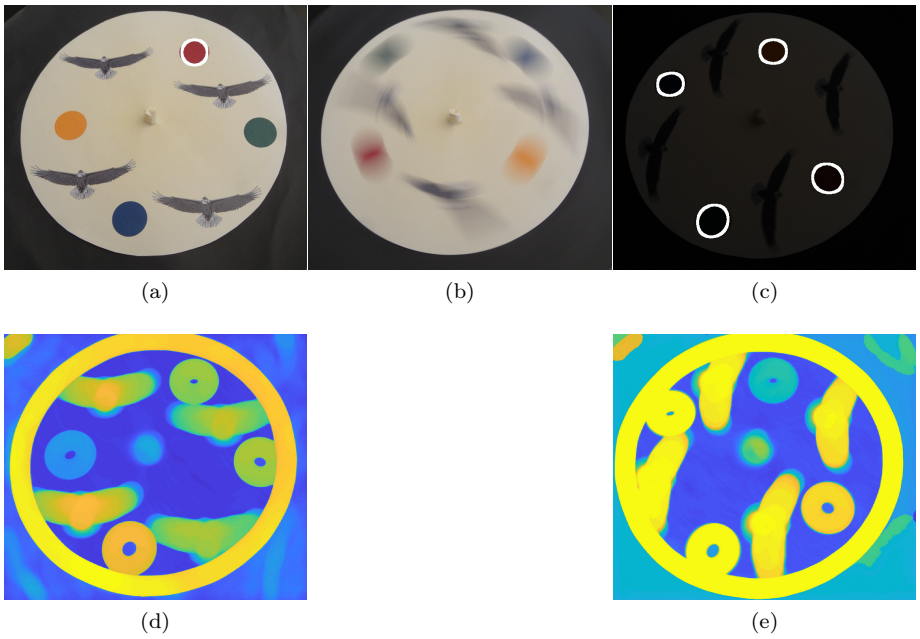

Figure 11: (a) Image f of the fixed object acquired with an exposure-time of 1/13 s. The probe function b is delineated in white. (d) Map of Asplund's distances $As^{\triangle}_{b^c,p}f^c$ of the complement of f. (b) Blurred image $f_{mov,bl}$ of the moving object acquired with the same exposure-time of 1/13 s. (c) Dark image $f_{mov,dk}$ of the moving object acquired with a short exposure-time of 1/160 s. The balls (delineated in white) are detected by finding the regional minima of its (e) map of LIP-additive Asplund's distances $As^{\triangle}_{b^c,p}f^c_{mov,dk}$. For each map, the tolerance parameter p is set to 95%.

circular, etc.) whose speed varies with the production rate.

6.3.2. LIP-multiplicative metric: images acquired with a variable absorption of the medium

The independence of the map of LIP-multiplicative Asplund's distances to light variations due to different absorption (or opacity) of the object is verified with a montage we made. It is composed of a transparent tank. On one of its sides a paper with motives is stuck. On the opposite side, a camera is disposed to capture an image of the paper through a medium composed of the tank and its contents: a green colourant diluted into water. Three images f_Γ (Fig. 12a), $f_{3\Gamma}$ (Fig. 12b) and $f_{12\Gamma}$ (Fig. 12c) are acquired for increasing concentrations of the colourant: Γ, 3Γ and 12Γ. One can notice that the image brightness decreases with the increase of the colourant concentration. A circular probe b is manually selected in the brightest image f_Γ in order to detect similar shapes in the two other images $f_{3\Gamma}$ and $f_{12\Gamma}$. A map of Asplund's distances is computed on the complement of each image with the same probe b and the same tolerance parameter $p = 90\%$. One can notice that the three maps of images

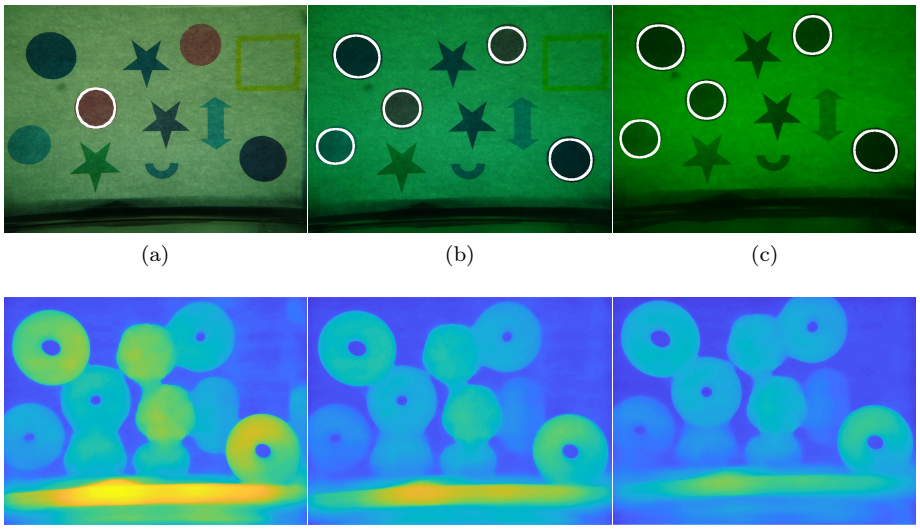

(a) (b) (c)

(d) (e) (f)

Figure 12: (a) Image f_Γ acquired with a small concentration, Γ, of colourant. The probe function b is delineated in white. (b) Ball detection in an image $f_{3\Gamma}$ acquired with an intermediate concentration, 3Γ, of colourant. (c) Ball detection in an image $f_{12\Gamma}$ acquired with a high concentration - 12Γ - of colourant. (d) Map of LIP-multiplicative Asplund's distances $As^{\triangle}_{b^c,p} f^c_\Gamma$ of the image f_Γ. (e) Map $As^{\triangle}_{b^c,p} f^c_{3\Gamma}$ of the image $f_{3\Gamma}$. (f) Map $As^{\triangle}_{b^c,p} f^c_{12\Gamma}$ of the image $f_{12\Gamma}$. The tolerance parameter p is set to 90 %.

$As^{\triangle}_{b^c,p} f^c_\Gamma$ (Fig. 12d), $As^{\triangle}_{b^c,p} f^c_{3\Gamma}$ (Fig. 12e) and $As^{\triangle}_{b^c,p} f^c_{12\Gamma}$ (Fig. 12f) present similar amplitudes. They are segmented by the same thresholding technique - at the 33^{rd} percentile - and two area openings in order to remove the too small and too large regions. The selected regions are then dilated for display purpose. One can notice that all the disks are detected in the two darkest images $f_{3\Gamma}$ (Fig. 12b) and $f_{12\Gamma}$ (Fig. 12c) using the probe b extracted in the bright image f_Γ. These results show the low sensitivity of the maps of LIP-multiplicative Asplund's distances to light variations caused by different absorptions. Such a situation occurs in images acquired by transmission (e.g. X-rays, tomography, spectrophotometry, etc.) [27].

Remark 14. In this section, probes with a circular invariance have been used to facilitate the presentation. However the Asplund's metrics are also efficient to detect non-circular objects with adapted probes. In addition, these metrics could be compared to the SIFT detector which is robust to lighting variations. The comparison has not been done in the sequel, because the robustness to lighting variations of the SIFT detector is not based on a physical law contrary to the Asplund's metrics. However, Noyel et al. [16] have shown that enhancing the contrast of images improves registration methods based on SIFT points [62]. We could therefore develop a SIFT in the LIP framework. These findings will be the studied in a future paper.

7. Conclusion

We have therefore successfully presented a new framework of pattern matching robust to lighting variations between low-contrast and high-contrast images. It is composed of two metrics. Firstly, the LIP-multiplicative Asplund's metric is robust to illumination changes due to variations of the object absorption or opacity. Secondly, the LIP-additive Asplund's metric is robust to illumination changes caused by variations of the source intensity or of the camera exposure-time. Both metrics are respectively based on the multiplicative and the additive laws of the LIP model which give them strong optical properties. Both functional metrics are thereby theoretically *insensitive to specific lighting variations*. They extend to images the property of *insensitivity to object magnification* of the Asplund's metric between binary shapes [23, 24]. After a presentation of the functional metrics and their properties, we have introduced robust to noise versions. We have demonstrated that the maps of Asplund's distances between an image and a probe function are composed of Mathematical Morphology operations. Both maps of distances are especially related to the morphological operations of dilations and erosions for functions. Such a relation facilitates the programming of the maps of distances because these operations exist in numerous image processing libraries. The properties of both metrics have been then verified with simulated and real cases. Results have shown that the maps of LIP-multiplicative and LIP-additive Asplund's distances are able to detect patterns in images acquired with different illuminations, caused by a stronger absorption of the object or by a shorter camera exposure-time, respectively. Importantly, the probe can be extracted in a highly contrasted image and the detection performed in a lowly contrasted image. Such properties pave the way to numerous applications where illumination variations are not controlled: e.g. in industry [61], medicine [63, 16], traffic control [64], safety and surveillance [8], imaging of moving objects [60], etc. In the future, these metrics will be extended to the analysis of colour and multivariate images starting from the preliminary ideas developed by Noyel and Jourlin [55, 65].

Appendix A.

The appendix is organised as follows. We will present the proofs of the propositions related to the LIP-multiplicative Asplund's metric (Prop. 1 and 5) and to the LIP-additive metric (Prop. 6, 7, 8 and 9).

Appendix A.1. Proofs of propositions 1 and 5 related to the LIP-multiplicative Asplund's metric

Proof of proposition 1, p. 9. c_1 and c_2 can be expressed as: $c_1 = \vee_{x\in D}\{\gamma(x)\}$ and $c_2 = \wedge_{x\in D}\{\gamma(x)\}$ with the function $\gamma = f \triangleq g, \gamma \in \mathcal{F}_M =]-\infty, M[^D$. There always exists a constant $k = \wedge_{x\in D}\{\gamma(x)\}$ such that $\gamma \triangleq k$ lies in $\mathcal{I} = [0, M[^D$ and thus is an image. Let us define $c_1^k = \vee_{x\in D}\{\gamma(x) \triangleq k\}$ and $c_2^k = \wedge_{x\in D}\{\gamma(x) \triangleq k\}$. c_1^k and c_2^k lie in $[0, M[$ and $c_1^k \geq c_2^k$. There is: $d^{\triangleq}_{As}(f, g) = \vee_{x\in D}\{\gamma(x)\} \triangleq \wedge_{x\in D}\{\gamma(x)\} =$

$\vee_{x\in D}\{\gamma(x) \triangle k\} \triangle \wedge_{x\in D}\{\gamma(x) \triangle k\} = c_1^k \triangle c_2^k$. Therefore, $d_{As}^{\triangleq}(f,g)$ lies in $[0, M[$ as the LIP-difference between c_1^k and $c_2^k \in [0, M[$, where $c_1^k \geq c_2^k$. □

Proof of proposition 5, p. 16 [35]. Let $f \in \overline{\mathcal{I}}$ be na image and $b \in \mathcal{T}^{D_b}$ be a probe. Using equations 15, 21 and 23 and knowing that $\tilde{f} \leq 0$, there is: $\forall x \in D$, $\lambda_b f(x) = \vee_{-h\in D_b}\{\tilde{f}(x-h)/\tilde{b}(-h)\}$. This leads to $\lambda_b f = (-\tilde{f})\dot{\oplus}(-1/\tilde{\tilde{b}}) = \exp(\ln(-\tilde{f}) \oplus (-\ln(-\tilde{\tilde{b}}))) = \exp(\hat{f} \oplus (-\hat{\tilde{b}}))$.
Similarly, there is $\mu_b f = (-\tilde{f})\dot{\ominus}(-\tilde{b}) = \exp[\hat{f} \ominus \hat{b}]$. The previous expressions of $\lambda_b f$ and $\mu_b f$ are used into equation 17 to obtain:
$As_b^{\triangleq} f = \ln(\exp[\hat{f} \oplus (-\hat{\tilde{b}})]/\exp[\hat{f} \ominus \hat{b})]) = [\hat{f} \oplus (-\hat{\tilde{b}})] - [\hat{f} \ominus \hat{b}] = \delta_{-\hat{\tilde{b}}}\hat{f} - \varepsilon_{\hat{b}}\hat{f}$.
□

Appendix A.2. Proofs of propositions 6, 7, 8 and 9 related to the LIP-additive Asplund's metric

Proof of proposition 6, p. 19. $\forall x \in D, \forall h \in D_b, \forall c \in \mathcal{F}_M$, there is: $c(x) \triangleq b(h) \geq f(x+h) \Leftrightarrow c(x) \geq f(x+h) \triangle b(h)$.

Equation 31 becomes therefore: $c_{1_b} f(x) = \inf\{c(x), c(x) \geq f(x+h) \triangle b(h), h \in D_b\} = \vee\{f(x+h) \triangle b(h), h \in D_b\}$. The last equality is due to the complete lattice structure. In a similar way, equation 32 becomes: $c_{2_b} f(x) = \sup\{c(x), c(x) \leq f(x+h) \triangle b(h), h \in D_b\} = \wedge\{f(x+h) \triangle b(h), h \in D_b\}$. □

Proof of proposition 7, p. 19. Let $b = b_0 \in (\mathcal{T})^{D_b}$ be a flat structuring element ($\forall x \in D_b$, $b(x) = b_0$). Knowing that $\triangle b_0$ preserves the order $\leq$ (i.e. it is an increasing operator), equations 33 of c_{1_b} and 34 of c_{2_b} can be simplified: $\forall x \in D$, $c_{1_{b_0}} f(x) = \vee\{f(x+h) \triangle b_0, h \in D_b\} = \vee\{f(x-h), -h \in D_b\} \triangle b_0 = \delta_{\overline{D}_b} f(x) \triangle b_0$. Similarly, $c_{2_{b_0}} f(x) = \wedge\{f(x+h), h \in D_b\} \triangle b_0 = \varepsilon_{D_b} f(x) \triangle b_0$. Equation 38, of the map of distances, is deduced from equation 35 and the expressions of $c_{1_{b_0}} f$ and $c_{2_{b_0}} f$. □

Proof of proposition 8, p. 20. As $\triangle b(h)$ preserves the order $\leq$ (i.e. it is an increasing operator), there is:
$\forall f, g \in \overline{\mathcal{F}}_M$, $\forall x \in D$, $c_{1_b}(f \vee g)(x) = \vee_{h\in D_b}\{((f \vee g)(x+h)) \triangle b(h)\} = \vee_{h\in D_b}\{(f(x+h) \triangle b(h)) \vee (g(x+h) \triangle b(h))\} = [\vee_{h\in D_b}\{f(x+h) \triangle b(h)\}] \vee [\vee_{h\in D_b}\{g(x+h) \triangle b(h)\}] = c_{1_b} f(x) \vee c_{1_b} g(x)$. In addition, $\forall x \in D$,
$c_{1_b}(O)(x) = c_{1_b}(f_{-\infty})(x) = \wedge_{h\in D_b}\{c(x), c(x) \geq (-\infty(x+h) \triangle b(h))\} =$
$\wedge_{h\in D_b}\{c(x), c(x) \geq M\frac{-\infty - b(h)}{M - b(h)}\} = -\infty = O(x)$, because $b(h) \in]-\infty, M[$. Therefore c_{1_b} is a dilation (Def. 4.2, p. 10).

Similarly, $\forall f, g \in \overline{\mathcal{F}}_M$, $c_{2_b}(f \wedge g) = c_{2_b}(f) \wedge c_{2_b}(g)$. In addition, $\forall x \in D$, $c_{2_b}(I)(x) = c_{2_b}(f_M)(x) = \vee_{h\in D_b}\{c(x), c(x) \leq M(x+h) \triangle b(h)\} = \vee_{h\in D_b}\{c(x), c(x) \leq M\frac{M - b(h)}{M - b(h)}\} = \vee_{h\in D_b}\{c(x), c(x) \leq M\} = M = I(x)$. Therefore, c_{2_b} is an erosion (Def. 4.1, p. 10).

□

Proof of proposition 9, p. 20. Let $f, g \in \overline{\mathcal{F}}_M$ be two functions. There is:
$\xi(f \triangleq g) = -M \ln(1 - (f \triangleq g)/M) = -M \ln((1 - f/M)(1 - g/M)) =$

$-M\ln(1-f/M)-M\ln(1-g/M)=\xi(f)+\xi(g)$, $\xi(\triangle g)=-M\ln(1+g/(M-g))=-M\ln(M/(M-g))=M\ln(1-g/M)=-\xi(g)$, and $\xi(f\triangle g)=\xi(f\triangleq(\triangle g))=\xi(f)+\xi(\triangle g)=\xi(f)-\xi(g)$ □

Appendix B. Supplementary materials

The supplementary materials to this article include: i) a video abstract, ii) the proofs of propositions 2, 3 and 4, iii) the verification of the properties of the LIP-additive Asplund's metric, iv) the proofs of the robust to noise metric invariances and v) details about the illustration section.

Appendix C. Acknowledgements

The authors thank Michel Smans for his technical support for the experiment of the figure 11.

[1] J. Li, B.-L. Lu, An adaptive image Euclidean distance, Pattern Recogn 42 (2009) 349 – 357. doi:10.1016/j.patcog.2008.07.017.

[2] L. Wang, Y. Zhang, J. Feng, On the Euclidean distance of images, IEEE T Pattern Anal 27 (2005) 1334–1339. doi:10.1109/TPAMI.2005.165.

[3] M. M. Deza, E. Deza, Encyclopedia of Distances, Springer Berlin Heidelberg, 2016. doi:10.1007/978-3-662-52844-0.

[4] E. R. Dougherty, Application of the hausdorff metric in gray-scale mathematical morphology via truncated umbrae, J Vis Commun Image R 2 (1991) 177–187. doi:10.1016/1047-3203(91)90007-3.

[5] D. P. Huttenlocher, G. A. Klanderman, W. J. Rucklidge, Comparing images using the hausdorff distance, IEEE T Pattern Anal 15 (1993) 850–863. doi:10.1109/34.232073.

[6] S. Messelodi, C. M. Modena, N. Segata, M. Zanin, A kalman filter based background updating algorithm robust to sharp illumination changes, in: Lect Notes Comput Sc, volume 3617, Springer, Berlin, Heidelberg, 2005, pp. 163–170. doi:10.1007/11553595_20.

[7] S. Salti, A. Petrelli, F. Tombari, N. Fioraio, L. D. Stefano, Traffic sign detection via interest region extraction, Pattern Recogn 48 (2015) 1039 – 1049. doi:10.1016/j.patcog.2014.05.017.

[8] G. L. Foresti, C. Micheloni, L. Snidaro, P. Remagnino, T. Ellis, Active video-based surveillance system: the low-level image and video processing techniques needed for implementation, IEEE Signal Proc Mag 22 (2005) 25–37. doi:10.1109/MSP.2005.1406473.

[9] Y.-T. Peng, P. C. Cosman, Underwater image restoration based on image blurriness and light absorption, IEEE T Image Process 26 (2017) 1579–1594. doi:10.1109/TIP.2017.2663846.

[10] C. O. Ancuti, C. Ancuti, C. De Vleeschouwer, P. Bekaert, Color balance and fusion for underwater image enhancement, IEEE T Image Process 27 (2018) 379–393. doi:10.1109/TIP.2017.2759252.

[11] N. Hautière, R. Labayrade, D. Aubert, Real-time disparity contrast combination for onboard estimation of the visibility distance, IEEE T Intell Transp 7 (2006) 201–212. doi:10.1109/TITS.2006.874682.

[12] W. Chen, M. J. Er, S. Wu, Illumination compensation and normalization for robust face recognition using discrete cosine transform in logarithm domain, IEEE T Syst Man Cy B 36 (2006) 458–466. doi:10.1109/TSMCB.2005.857353.

[13] M. R. Faraji, X. Qi, Face recognition under varying illuminations using logarithmic fractal dimension-based complete eight local directional patterns, Neurocomputing 199 (2016) 16–30. doi:10.1016/j.neucom.2016.01.094.

[14] J. Hussain Shah, M. Sharif, M. Raza, M. Murtaza, S. Ur-Rehman, Robust face recognition technique under varying illumination, J Appl Res Technol 13 (2015) 97–105. doi:10.1016/S1665-6423(15)30008-0.

[15] Z.-R. Lai, D.-Q. Dai, C.-X. Ren, K.-K. Huang, Multilayer surface albedo for face recognition with reference images in bad lighting conditions, IEEE T Image Process 23 (2014) 4709–4723. doi:10.1109/TIP.2014.2356292.

[16] G. Noyel, R. Thomas, G. Bhakta, A. Crowder, D. Owens, P. Boyle, Superimposition of eye fundus images for longitudinal analysis from large public health databases, Biomed Phys Eng Express 3 (2017) 045015. doi:10.1088/2057-1976/aa7d16.

[17] S. Shan, W. Gao, B. Cao, D. Zhao, Illumination normalization for robust face recognition against varying lighting conditions, in: IEEE Int SOI Conf, 2003, pp. 157–164. doi:10.1109/AMFG.2003.1240838.

[18] M. Savvides, B. V. Kumar, Illumination normalization using logarithm transforms for face authentication, in: Lect Notes Comp Sc, volume 2688, Springer Berlin Heidelberg, 2003, pp. 549–556. doi:10.1007/3-540-44887-X_65.

[19] S. M. Pizer, E. P. Amburn, J. D. Austin, R. Cromartie, A. Geselowitz, T. Greer, B. ter Haar Romeny, J. B. Zimmerman, K. Zuiderveld, Adaptive histogram equalization and its variations, Comput Vis, Graph, Image Process 39 (1987) 355 – 368. doi:10.1016/S0734-189X(87)80186-X.

[20] X. Xie, K.-M. Lam, Face recognition under varying illumination based on a 2d face shape model, Pattern Recogn 38 (2005) 221 – 230. doi:10.1016/j.patcog.2004.07.002.

[21] G. Deng, A generalized unsharp masking algorithm, IEEE T Image Process 20 (2011) 1249–1261. doi:10.1109/TIP.2010.2092441.

[22] L. Meylan, S. Susstrunk, High dynamic range image rendering with a retinex-based adaptive filter, IEEE T Image Process 15 (2006) 2820–2830. doi:10.1109/TIP.2006.877312.

[23] E. Asplund, Comparison Between Plane Symmetric Convex Bodies and Parallelograms., Math Scand 8 (1960) 171–180. doi:10.7146/math.scand.a-10606.

[24] B. Grünbaum, Measures of symmetry for convex sets, in: P Symp Pure Math, volume 7, Amer. Math. Soc., Providence, R.I., 1963, pp. 233–270. doi:10.1090/pspum/007.

[25] M. Jourlin, E. Couka, B. Abdallah, J. Corvo, J. Breugnot, Asplünd's metric defined in the Logarithmic Image Processing (LIP) framework: A new way to perform double-sided image probing for non-linear grayscale pattern matching, Pattern Recogn 47 (2014) 2908 – 2924. doi:10.1016/j.patcog.2014.03.031.

[26] M. Jourlin, J. Pinoli, Logarithmic image processing: The mathematical and physical framework for the representation and processing of transmitted images, in: Adv Imag Elect Phys, volume 115, Elsevier, 2001, pp. 129 – 196. doi:10.1016/S1076-5670(01)80095-1.

[27] M. Jourlin, Logarithmic Image Processing: Theory and Applications, volume 195 of *Adv Imag Elect Phys*, Elsevier Science, 2016. doi:10.1016/S1076-5670(16)30078-7.

[28] G. Matheron, Eléments pour une théorie des milieux poreux, Masson, Paris, 1967.

[29] J. Serra, N. Cressie, Image Analysis and Mathematical Morphology, volume 1, Academic Press, New York, 1982.

[30] H. Heijmans, Morphological image operators, number vol. 25 in Adv Imag Elect Phys: Supplement, Academic Press, 1994.

[31] L. Najman, H. Talbot, Mathematical Morphology: From Theory to Applications, 1 ed., Wiley-Blackwell, 2013. doi:10.1002/9781118600788.

[32] J. Brailean, B. Sullivan, C. Chen, M. Giger, Evaluating the EM algorithm for image processing using a human visual fidelity criterion, in: Int Conf Acoust Spee, 1991, pp. 2957–2960 vol.4. doi:10.1109/ICASSP.1991.151023.

[33] M. Jourlin, M. Carré, J. Breugnot, M. Bouabdellah, Chapter 7 - Logarithmic image processing: Additive contrast, multiplicative contrast, and associated metrics, in: Adv Imag Elect Phys, volume 171, Elsevier, 2012, pp. 357 – 406. doi:10.1016/B978-0-12-394297-5.00007-6.

[34] G. Noyel, M. Jourlin, Double-sided probing by map of Asplund's distances using logarithmic image processing in the framework of mathematical morphology, in: Lect Notes Comput Sc, volume 10225, Springer Int Publishing, Cham, 2017, pp. 408–420. doi:10.1007/978-3-319-57240-6_33.

[35] G. Noyel, M. Jourlin, A simple expression for the map of Asplund's distances with the multiplicative Logarithmic Image Processing (LIP) law, 2017. URL: https://arxiv.org/abs/1708.08992, personal communication, Eur Congr Stereology and Image Anal, Kaiserslautern, Germany.

[36] G. Noyel, Logarithmic mathematical morphology: A new framework adaptive to illumination changes, in: Lect Notes Comp Sc, volume 11401, Springer Int Publishing, Cham, 2019, pp. 453–461. doi:10.1007/978-3-030-13469-3_53.

[37] C. Barat, C. Ducottet, M. Jourlin, Pattern matching using morphological probing, in: IEEE Image Proc, volume 1, 2003, pp. I–369–72. doi:10.1109/ICIP.2003.1246975.

[38] C. Barat, C. Ducottet, M. Jourlin, Virtual double-sided image probing: A unifying framework for non-linear grayscale pattern matching, Pattern Recogn 43 (2010) 3433–3447. doi:10.1016/j.patcog.2010.04.020.

[39] G. Banon, S. Faria, Morphological approach for template matching, in: Proc. X Brazilian Symp. on Comput. Graphics and Image Process., 1997, pp. 171–178. doi:10.1109/SIGRA.1997.625169.

[40] M. Khosravi, R. Schafer, Template matching based on a grayscale hit-or-miss transform, IEEE T Image Process 5 (1996) 1060–1066. doi:10.1109/83.503921.

[41] F. Odone, E. Trucco, A. Verri, General purpose matching of grey level arbitrary images, in: Lect Notes Comput Sc, volume 2059, Springer, Berlin, Heidelberg, 2001, pp. 573–582. doi:10.1007/3-540-45129-3_53.

[42] V. Cantoni, L. Cinque, C. Guerra, S. Levialdi, L. Lombardi, 2-D object recognition by multiscale tree matching, Pattern Recogn 31 (1998) 1443 – 1454. doi:10.1016/S0031-3203(97)00085-X.

[43] M. Jourlin, J. Pinoli, A model for logarithmic image-processing, J Microsc-Oxford 149 (1988) 21–35. doi:10.1111/j.1365-2818.1988.tb04559.x.

[44] M. Carre, M. Jourlin, LIP operators: Simulating exposure variations to perform algorithms independent of lighting conditions, in: Int Conf on Multimedia Computing and Syst (ICMCS), 2014, pp. 122–126. doi:10.1109/ICMCS.2014.6911247.

[45] V. Deshayes, P. Guilbert, M. Jourlin, How simulating exposure time variations in the LIP model. application: moving objects acquisition, in: Acta Stereol., Proc. 14th ICSIA, 2015. URL: https://popups.uliege.be:443/0351-580X/index.php?id=3663.

[46] F. Mayet, J.-C. Pinoli, M. Jourlin, Physical justifications and applications of the LIP model for the processing of transmitted light images, Trait Signal 13 (1996) 251 – 262. URL: http://hdl.handle.net/2042/1959.

[47] L. Navarro, G. Deng, G. Courbebaisse, The symmetric logarithmic image processing model, Digital Signal Process 23 (2013) 1337 – 1343. doi:10.1016/j.dsp.2013.07.001.

[48] L. Navarro, G. Courbebaisse, M. Jourlin, Chapter two - Logarithmic wavelets, volume 183 of *Adv Imag Elect Phy*, Elsevier, 2014, pp. 41 – 98. doi:https://doi.org/10.1016/B978-0-12-800265-0.00002-3.

[49] H. Heijmans, C. Ronse, The algebraic basis of mathematical morphology I. dilations and erosions, Comput Vision Graphics and Image Process 50 (1990) 245 – 295. doi:10.1016/0734-189X(90)90148-O.

[50] P. Soille, Morphological Image Analysis: Principles and Applications, 2 ed., Springer, Berlin, Heidelberg, 2004. doi:10.1007/978-3-662-05088-0.

[51] N. Bouaynaya, D. Schonfeld, Theoretical foundations of spatially-variant mathematical morphology part II: Gray-level images, IEEE T Pattern Anal 30 (2008) 837–850. doi:10.1109/TPAMI.2007.70756.

[52] J. J. van de Gronde, J. B. T. M. Roerdink, Group-invariant colour morphology based on frames, IEEE T Image Process 23 (2014) 1276–1288. doi:10.1109/TIP.2014.2300816.

[53] G. J. F. Banon, J. Barrera, Decomposition of mappings between complete lattices by mathematical morphology, part I: General lattices, Signal Process 30 (1993) 299 – 327. doi:10.1016/0165-1684(93)90015-3.

[54] J. Serra, Image analysis and mathematical morphology: Theoretical advances, volume 2, Academic Press, 1988.

[55] G. Noyel, M. Jourlin, Asplund's metric defined in the logarithmic image processing (LIP) framework for colour and multivariate images, in: IEEE Image Proc, 2015, pp. 3921–3925. doi:10.1109/ICIP.2015.7351540.

[56] Butterfly, Image from the YFCC100M dataset, http://www.flickr.com/photos/45563311@N04/4350683057/, 2010. Licence CC BY-NC-SA 2.0.

[57] B. Thomee, D. A. Shamma, G. Friedland, B. Elizalde, K. Ni, D. Poland, D. Borth, L.-J. Li, YFCC100M: The new data in multimedia research, Commun ACM 59 (2016) 64–73. doi:10.1145/2812802.

[58] N. Bourbaki, Intégration: Chapitres 1 à 4, Bourbaki, Nicolas, Springer Berlin Heidelberg, 2007. doi:10.1007/978-3-540-35329-4.

[59] M. Jourlin, J.-C. Pinoli, Image dynamic range enhancement and stabilization in the context of the logarithmic image processing model, Signal Process 41 (1995) 225 – 237. doi:10.1016/0165-1684(94)00102-6.

[60] G. Noyel, Method of monitoring the appearance of the surface of a tire, https://patentscope.wipo.int/search/en/WO2011131410, 2011. Patent, International PCT no WO2011131410 (A1). Also published as: US9002093 (B2), FR2959046 (B1), JP5779232 (B2), EP2561479 (A1), CN102844791 (B), BR112012025402 (A2).

[61] G. Noyel, D. Jeulin, E. Parra-Denis, M. Bilodeau, Method of checking the appearance of the surface of a tyre, https://patentscope.wipo.int/search/en/WO2013045593, 2013. Patent, International PCT no WO2013045593 (A1), also published as US9189841 (B2), FR2980735 (B1), EP2761587 (A1), CN103843034 (A).

[62] D. G. Lowe, Distinctive image features from scale-invariant keypoints, Int J Comput Vision 60 (2004) 91–110. URL: https://doi.org/10.1023/B:VISI.0000029664.99615.94. doi:10.1023/B:VISI.0000029664.99615.94.

[63] G. Noyel, J. Angulo, D. Jeulin, D. Balvay, C.-A. Cuenod, Multivariate mathematical morphology for DCE-MRI image analysis in angiogenesis studies, Image Anal Stereol 34 (2014) 1–25.

[64] A. Geiger, M. Lauer, C. Wojek, C. Stiller, R. Urtasun, 3d traffic scene understanding from movable platforms, IEEE T Pattern Anal 36 (2014) 1012–1025. doi:10.1109/TPAMI.2013.185.

[65] G. Noyel, M. Jourlin, Spatio-colour Asplünd's metric and logarithmic image processing for colour images (LIPC), in: Lect Notes Comp Sc, volume 10125, Springer, Cham, 2017, pp. 36–43. doi:10.1007/978-3-319-52277-7_5.